A rational chemical optimization framework to enhance shoot regeneration capacity in plants

Guan-Dong Shang[1,2#], Fu-Xiang Wang[1#], Heng Lian[1], Si-Yu Wang[1,3], Lian-Yu Wu[1], Zhou-Geng Xu[1], Si-Qin Lv[1], Bei Li[1,4], Jia-Wei Wang[*1,5,6]

Callus refers to a mass of undifferentiated cells formed from explants at sites of injury or in tissue culture. As genome-editing technologies advance, enhancing the shoot regeneration capacity of callus is increasingly critical for crop improvement. Here, we demonstrate that shoot regeneration competence is restricted to discrete cellular states within *Arabidopsis* callus, resulting in the widespread formation of ineffective callus regions. Building on this insight, we establish a four-step framework to enhance regeneration capacity, encompassing spatiotemporal transcriptomic profiling of callus development, identification of ineffective callus regions and their molecular markers, reporter-based high-throughput chemical screening, and the rational selection of individual compounds. Using this strategy, we identify the MEK inhibitor U0126 as a potent regulator that markedly reduces ineffective callus regions via the MKK4/5–MPK3/6 pathway and enhances shoot regeneration across multiple dicotyledonous and monocotyledonous species. Together, these findings define a conceptually advanced alternative to traditional trial-and-error approaches for regeneration optimization.

https://doi.org/10.15302/vita.2026.10.0086

INTRODUCTION

Plants exhibit remarkable regenerative capabilities[1-4], with somatic cells in specific lineages retaining pluripotency and the potential to regenerate shoots or roots under appropriate conditions[5-11]. Plant regeneration is vital for generating genome-edited and transgenic crops, but current methods require improvement to enhance regeneration capacity across diverse species and genotypes[12,13].

Callus, a proliferating, partially dedifferentiated, and developmentally plastic cellular population induced by wounding or tissue culture conditions[14], is critical in regeneration protocols. In the widely used two-step tissue culture system, explants are cultured on auxin-rich callus-inducing medium (CIM) to generate pluripotent callus[14,15], then transferred to cytokinin-rich shoot-inducing medium (SIM) for shoot induction[2,6,16]. In *Arabidopsis thaliana*, callus originates from pericycle and pericycle-like cells, with auxin playing a pivotal role[17-19]. Mutations in *Aberrant Lateral Root Formation 4* (*ALF4*) block pericycle division, inhibiting callus formation on the CIM[20-22]. Conversely, overexpression of the DNA binding with one finger (DOF) transcription factor *OBF Binding Protein 4* (*OBP4*) promotes pericycle proliferation, leading to the formation of callus-like structures at root tips[23]. Very long-chain fatty acids (VLCFAs) restrict pericycle competence for callus formation by acting as cell-layer signals[24].

Inactivation of *CALLUS FORMATION RELATED 1* (*CFR1*), encoding a rate-limiting enzyme, 3-ketoacyl-CoA synthase, in the VLCFA biosynthesis pathway, allows pericycle cell division and callus formation even in the presence of auxin signaling pathway defects. Calcium signaling also mediates callus formation, where the CALMODULIN IQ-MOTIF CONTAINING PROTEIN (CaM-IQM) complex interacts with auxin signaling repressors in a Ca^{2+}-dependent manner[25]. For instance, CaM6–IAA19 interaction releases IAA19 inhibition on AUXIN RESPONSE FACTORs 7 and 19 (ARF7/19), key transcription factors for callus initiation.

Auxin regulates callus formation via the bZIP59–LBD complex in *A. thaliana*[26]. ARF7/19 induce expression of LBD16, LBD17, LBD18, and LBD29, while auxin stabilizes bZIP59 to enhance interaction with LBDs[27]. This complex promotes callus formation by activating cell wall metabolism genes, such as *FAD-BD*. Disruptions in bZIP59 or LBDs reduce auxin-induced callus formation. Other factors, including WRKY23 and bHLH041, act downstream of ARF7/19 to establish callus pluripotency[28].

In addition to stimulating cell proliferation of the callus, auxin induces pluripotency on the CIM[29]. Transcriptome studies uncover that the callus shares characteristics with root developmental pathways, as root meristem genes like *WUSCHEL RELATED HOMEOBOX 5* (*WOX5*), *SCARECROW* (*SCR*), and *SHORT ROOT* (*SHR*) are ectopically expressed in callus[22,30]. AP2-family transcription factors (e.g., PLETHORA3 (PLT3), PLT5, PLT7) reprogram callus cells into a pluripotent state by activating *PLT1/2* and *NAC*-family genes *CUC1* and

1. Key Laboratory of Plant Carbon Capture, CAS Center for Excellence in Molecular Plant Sciences (CEMPS), Institute of Plant Physiology and Ecology (SIPPE), Chinese Academy of Sciences (CAS), Shanghai, China. 2. Biotechnology Institute, Xianghu Laboratory, Hangzhou, Zhejiang, China. 3. University of Chinese Academy of Sciences (UCAS), Shanghai, China. 4. Core Facility Center of CEMPS, SIPPE, CAS, Shanghai, China. 5. School of Life Science and Technology, ShanghaiTech University, Shanghai, China. 6. New Cornerstone Science Laboratory, Shanghai, China. #These two authors contribute equally. *Correspondence: Jia-Wei Wang (jwwang@sippe.ac.cn)

Received: June 2, 2026; Accepted: October 23, 2026; Published: November 10, 2026

CUC2[29]. Mutations in *PLT3*, *PLT5*, and *PLT7* resulted in pronounced defects in callus formation and pluripotency. Three WOX-family TF genes also play important roles in pluripotency, with contrasting functions. While WOX11 functions by activating *LBD16*[31], WOX5 induces the expression of an auxin synthesis enzyme gene, *TRYPTOPHAN AMINOTRANSFERASE OF ARABIDOPSIS 1* (*TAA1*), through its interaction with PLT1 and PLT2[32]. Blocking these cascades leads to the loss of callus pluripotency on the CIM and impairs shoot formation on the SIM. Conversely, WOX13 negatively regulates shoot regeneration by promoting genes involved in cell expansion and cellular differentiation and repressing those associated with the shoot apical meristem (SAM)[33].

Epigenetic regulation is vital in callus formation[34,35]. DNA methylation, chromatin accessibility, histone modifications, and histone variants trigger dramatic dynamic changes during somatic cell reprogramming and pluripotency acquisition[36-42]. Mutants associated with DNA methylation and histone modifications display regeneration defects[37,43-45]. Not all callus cells are pluripotent, and single-cell RNA sequencing (scRNA-seq) studies have revealed cellular heterogeneity in *A. thaliana*[32,33,46]. Callus cells can be grouped into three cell layers along the direction perpendicular to the vascular bundle of the explant[32]. The middle layer, characterized by a transcriptional identity similar to the root quiescent center, can regenerate shoots.

In summary, significant progress has been made in uncovering the mechanisms driving callus induction and pluripotency acquisition on the CIM. However, despite the widespread presence of the middle layer within mature callus, it remains unclear why not all regions are equally effective for shoot regeneration. Addressing this question could further enhance shoot regeneration capacity, benefiting future crop design.

To investigate this, we created a comprehensive spatiotemporal cellular map of *A. thaliana* callus at single-cell resolution. We discovered that heterogeneity in cell division patterns leads to asynchronous callus development using approximately 40 cell type-specific fluorescent protein reporter lines and time-lapsed imaging. Notably, early-formed prominent protrusions were identified as ineffective regions predisposed to root development. Leveraging a gene signature associated with these ineffective regions and conducting a chemical screen, we identified U0126 as a compound significantly reducing ineffective callus regions and enhancing shoot regeneration across various dicotyledonous and monocotyledonous plants. Notably, these results establish an innovative chemical optimization framework for boosting regeneration capacity, representing a significant conceptual advancement over traditional trial-and-error approaches[13].

RESULTS

A time-resolved cell atlas of callus at single-cell resolution

Previous single-cell sequencing studies on *A. thaliana* callus derived from hypocotyls were limited to a single time point[32,33], providing minimal insight into the gradual emergence of new cell types during callus initiation and development. In this study, we used *A. thaliana* hypocotyls as explants and followed the regeneration protocol described by Wu *et al*.[38]. Explants (CIM0) and calli were sampled at three developmental stages (Fig. 1). On the CIM, pericycle cell division was evident as early as day 1 (CIM1). By day 3 (CIM3), one to five cell layers had formed, and by day 7 (CIM7), prominent callus protrusions were observed. Subsequent transfer of these calli onto the SIM induced shoot formation.

High-quality protoplasts were prepared, and single-cell transcriptome libraries were generated using the 10× Genomics Chromium scRNA-seq platform. The data were analyzed using published protocols (see Materials and Methods). Since tissue culture represents an unnatural growth condition, existing *A. thaliana* cell type markers derived from root and shoot scRNA-seq datasets[47-49] may not precisely annotate callus cell types. To address this, we conducted large-scale promoter-reporter analyses. Regulatory regions of top cluster-specific genes were cloned to generate Green Fluorescent Protein (GFP) or DsRed reporter lines. The spatial expression patterns of 39 reporter lines, combined with known cell type markers, allowed us to annotate cell clusters at each time point (Supplementary Figs. S1–S7 and Text S1). Overall, annotations at CIM0 were consistent with prior anatomical characterizations of *A. thaliana* hypocotyls (Fig. 1a)[50]. At CIM1 and CIM3, wound-responsive cells and nascent callus clusters were readily detected (Fig. 1b, c). By CIM7, in agreement with earlier reports, three distinct callus layers — outer, middle, and inner — were clearly resolved (Fig. 1d)[32,33]. Collectively, this time-resolved scRNA-seq analysis produced a comprehensive cellular atlas of *A. thaliana* callus, capturing dynamic shifts in cell identity throughout callus development.

Hidden cell heterogeneity revealed by spatial transcriptomics

During our observations, to our surprise, we found that several reporters exhibited spatial heterogeneity at CIM7, which does not simply conform to the three-layer principle of callus organization proposed by Zhai *et al*.[32]. For instance, *INDOLE-3-ACETIC ACID7* (*IAA7*, *AT3G23050*) and *AT2G22510* were expressed only in specific regions of the outer layer (Supplementary Fig. S4a), suggesting previously unrecognized spatial diversity. To validate this, we employed *in situ* RNA sequencing (IISS) (see Materials and Methods)[51], as commercial spatial transcriptomics platforms like 10× Genomics Visium, Curio Seeker, and Stereo-seq are unsuitable for the small tissue size of *A. thaliana* calli[52-55]. Based on our cell atlas annotations (Supplementary Table S1), we designed RNA probes for over 100 representative genes and generated a spatial transcriptomic map for the CIM7 callus.

To confirm the accuracy of this spatial map, we examined the localization of several known genes. For example, *ATML1* was expressed in the outer proliferating cell layer, while transcripts of *WOX5*, *PLT1*, *PLT2*, *TAA1*, and *SCR* were enriched in middle layers, and *SHR* was predominantly localized in inner layers (Fig. 2a; Supplementary Fig. S5a)[32,33]. In contrast, *PLT3* showed uniform expression across all proliferating cells[56], further corroborating the reliability of our spatial transcriptomics and single-cell annotations.

Through spatial analysis, we identified five novel cell types (N1 to N5) that could not be spatially resolved via scRNA-seq (Fig. 2b, c; Supplementary Fig. S4b). N1 and N2 cells were localized to the outermost layers of distinct callus regions: the flat callus region (FCR) and the arched callus region (ACR), respectively (Fig. 2b, c). While the epidermal marker *ATML1*

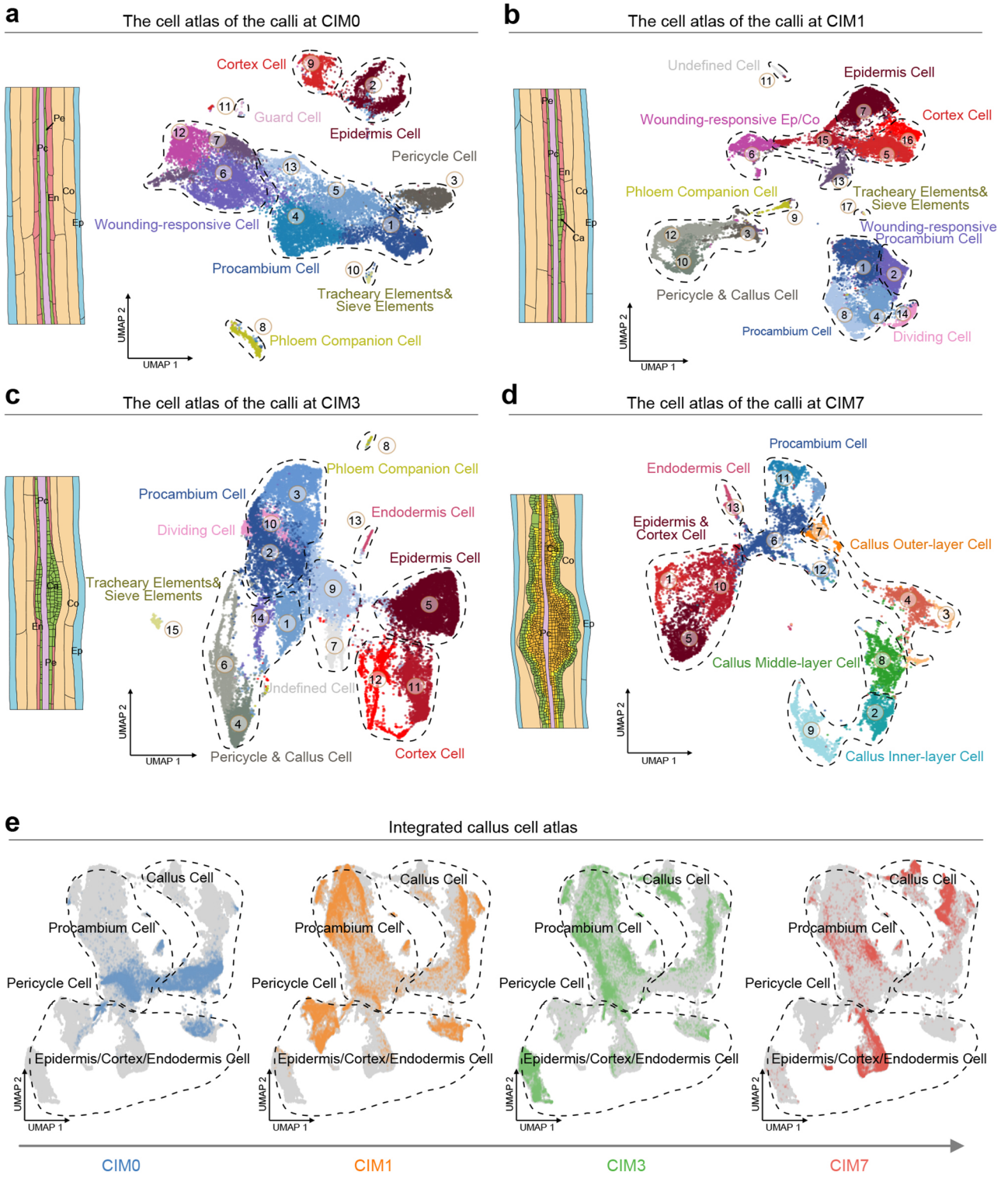


Fig. 1 Time-resolved callus cell atlas in *Arabidopsis*. **a**–**d** The cell atlases of the calli at CIM0 (**a**), CIM1 (**b**), CIM3 (**c**), and CIM7 (**d**). Schematic diagrams of calli at cellular resolution for each time point are shown on the left in each panel. Ca: callus cells; Co: cortex; En, endodermis; Ep: epidermis; Pe: pericycle; Pc, procambium. The atlases are visualized using UMAPs. Each dot represents a single cell, with different colors indicating distinct cell clusters. Clusters of the same cell type are outlined with dashed lines. Biological replicates: $n = 2$ for CIM0, $n = 2$ for CIM1, $n = 2$ for CIM3, and $n = 1$ for CIM7. **e** Integrated callus cell atlas. The atlases in **a**–**d** were merged to generate a time-resolved cell atlas of calli. The UMAP is colored by different time points (CIM0 to CIM7). Procambium and Epidermis/Cortex/Endodermis populations are outlined with dashed lines. See also Supplementary Figs. S1–S3.

failed to differentiate these populations, *LONG-CHAIN ACYL-COA SYNTHETASE 2* (*LACS2*), *GGL12*, and *CYP77B1* were preferentially expressed in the FCR, whereas *3-KETOACYL-COA SYNTHASE 16* (*KCS16*, *AT4G34250*) was principally restricted

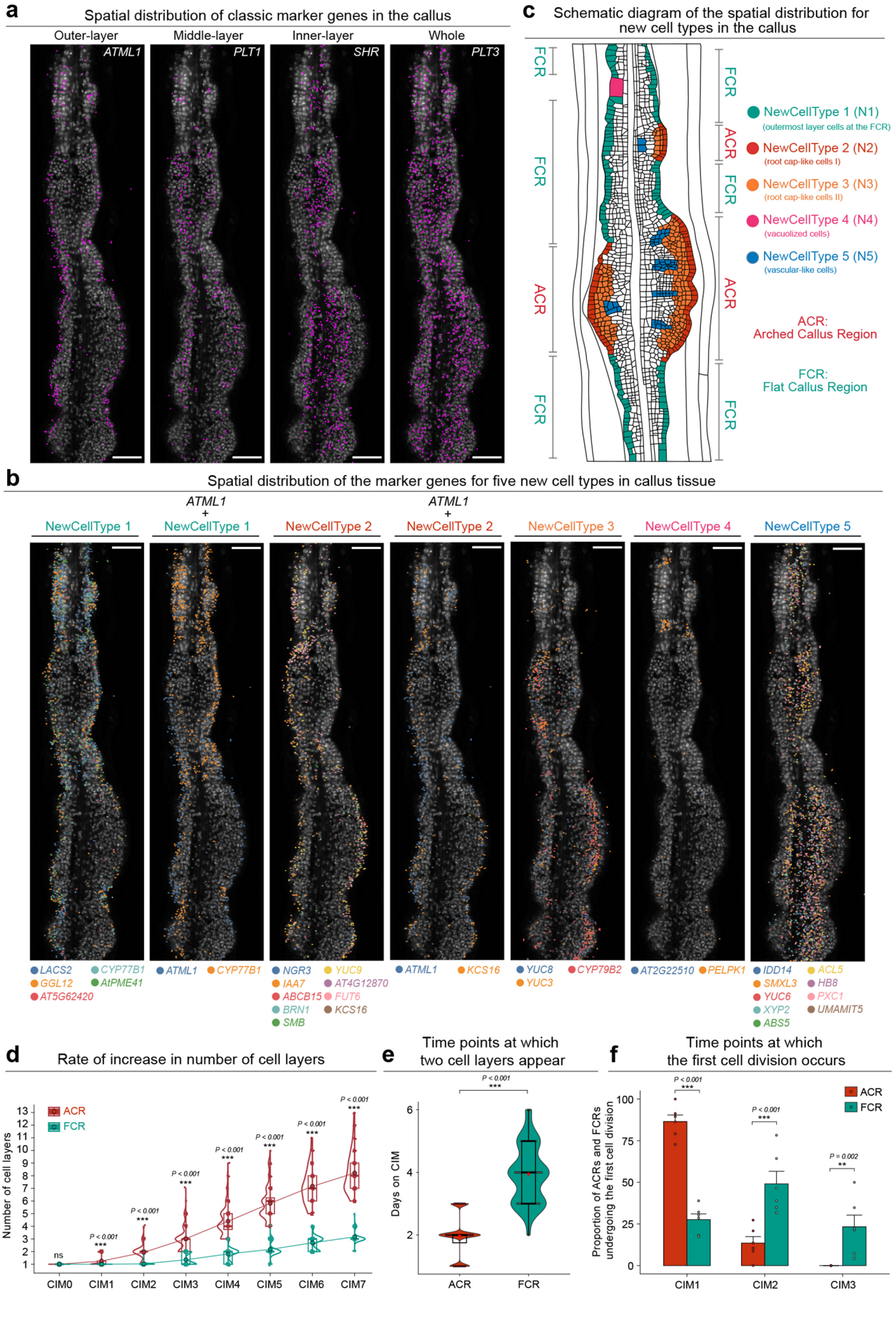

a
Spatial distribution of classic marker genes in the callus
Outer-layer
Middle-layer
Inner-layer
Whole
ATML1
PLT1
SHR
PLT3
c
Schematic diagram of the spatial distribution for new cell types in the callus
FCR
ACR
NewCellType 1 (N1)
(outermost layer cells at the FCR)
NewCellType 2 (N2)
(root cap-like cells I)
NewCellType 3 (N3)
(root cap-like cells II)
NewCellType 4 (N4)
(vacuolized cells)
NewCellType 5 (N5)
(vascular-like cells)
ACR:
Arched Callus Region
FCR:
Flat Callus Region
b
Spatial distribution of the marker genes for five new cell types in callus tissue
NewCellType 1
ATML1 + NewCellType 1
NewCellType 2
ATML1 + NewCellType 2
NewCellType 3
NewCellType 4
NewCellType 5
LACS2
CYP77B1
GGL12
AtPME41
AT5G62420
ATML1
CYP77B1
NGR3
YUC9
IAA7
AT4G12870
ABCB15
FUT6
BRN1
KCS16
SMB
ATML1
KCS16
YUC8
CYP79B2
YUC3
AT2G22510
PELPK1
IDD14
ACL5
SMXL3
HB8
YUC6
PXC1
XYP2
UMAMIT5
ABS5
d
Rate of increase in number of cell layers
ACR
FCR
Number of cell layers
P < 0.001
***
ns
CIM0
CIM1
CIM2
CIM3
CIM4
CIM5
CIM6
CIM7
e
Time points at which two cell layers appear
Days on CIM
ACR
FCR
f
Time points at which the first cell division occurs
Proportion of ACRs and FCRs undergoing the first cell division
P = 0.002
**
CIM1
CIM2
CIM3

Fig. 2 Spatial transcriptomics of calli at CIM7 and cell division tracking. a Spatial distribution of four classic marker genes in the callus. One representative gene for the outer layer, middle layer, inner layer, and whole callus tissue is shown. The purple dots represent regions of gene expression. Nuclei (grey) were stained with DAPI. Scale bars, 50 μm. **b** Spatial distribution of the marker genes for five new cell types (N1 to N5) in the callus. Gene names are shown at the bottom of each panel, with different colors denoting distinct genes. Scale bars, 50 μm. **c** Schematic diagram of the spatial distribution for new cell types in the callus. Two distinct callus regions, ACR and FCR, are illustrated. Note that new cell types (N2, N3, and N5) are primarily located in the ACR. **d** Rate of increase in cell layer number in ACRs and FCRs. Calli were monitored daily from CIM0 to CIM7 using a constitutive nuclear localization reporter (*pAT2G18020:H2B-mCherry*) (Supplementary Fig. S8a). Eight explants were analyzed and quantified. *n* represents the number of tracked callus regions (n = 104 for ACRs and n = 111 for FCRs). **e** Time points at which two distinct cell layers first appeared in ACRs and FCRs. The experimental setup was identical to that described in **d**. **f** Proportion of ACRs and FCRs undergoing their first cell division at different time points. G2–M signals in the corresponding pericycle cells, detected by Cytrap, served as indicators of mitotic entry (Supplementary Fig. S8b). Six explants were analyzed and quantified. *n* represents the number of tracked callus regions (n = 120 for ACRs and n = 128 for FCRs). Statistical analyses were performed using the generalized linear mixed model (GLMM) with a generalized Poisson distribution (**d**), a mixed-effects Cox proportional hazards model (**e**), and a linear mixed-effects model (LMM) (**f**). $^{***}P < 0.001$; $^{**}P < 0.01$; $^{*}P < 0.05$; ns, no significant difference. See also Supplementary Figs. S4–S8.

to the ACR (Fig. 2b; Supplementary Figs. S4b and S5b–d). These findings suggest that the outermost layers of these regions exhibit distinct surface characteristics, potentially reflecting differences in long-chain fatty acid composition. Other marker genes for N2 included *IAA7* and *ABCB15*. While *IAA7* was initially expressed in the epidermis and cortex during early callus development, its transcripts predominantly localized to the outermost cell layer of the ACR at CIM7 (Supplementary Fig. S5e, f). *ABCB15* displayed a similar expression pattern (Supplementary Fig. S5g).

In contrast, N3 cells were located in the L2–L5 layers of the ACR and marked by genes such as *YUCCA3* (*YUC3*), *YUC8*, and *CYP79B2* (Fig. 2b, c; Supplementary Figs. S4b, S6a, b). Interestingly, both N2 and N3 were parts of cluster 3 in the CIM7 cell atlas (Fig. 1d), indicating similar cellular states. Remarkably, several root cap genes, including *BEARSKIN 1* (*BRN1*), *BRN2*, and *SMB*[57] were highly enriched in cluster 3 at CIM7 and specifically expressed in N2 as shown by spatial transcriptomics (Fig. 2b; Supplementary Figs. S4b and S6c). Furthermore, the top marker genes of cluster 3 at CIM7 were significantly enriched in the root cap cluster from published root cell atlases (Supplementary Fig. S6d)[58]. These findings indicate that N2 and N3 in the ACR represent a unique cell type with root cap-like properties. Consequently, we designated N2 and N3 as the "root cap-like cells I and II", and N1 as the "outermost layer cells at the FCR".

N4 cells were identified using *AT2G22510* and *PRO-GLU-LEU|ILE|VAL-PRO-LYS 1* (*PELPK1*) as markers (Fig. 2b, c; Supplementary Figs. S4b and S6e–g). At CIM3, these cells (cluster 13 cells at the CIM3, Fig. 1c) were categorized as "overlying ground tissue cells" that are later penetrated by inner proliferating callus cells (Fig. 2b, c; Supplementary Fig. S6e–g). At CIM7, they (cluster 13 cells at the CIM7, Fig. 1d) maintained specific localization within the callus, exhibiting larger volumes compared to adjacent proliferating cells (Supplementary Fig. S6e–g). Notably, these cells were enriched in genes associated with cell death and senescence, including *BIFUNCTIONAL NUCLEASE 1* (*BFN1*), *SENESCENCE ASSOCIATED GENE 29* (*SAG29*), *RIBONUCLEASE 3* (*RNS3*), *METACASPASE 9* (*MC9*), *EXITUS 1* (*EXI1*), and *DUF679 DOMAIN MEMBRANE PROTEIN 4* (*DMP4*) (Supplementary Fig. S6h)[59,60].

A recent study by the Sugimoto and Ikeuchi labs identified "highly expanded globular cells" in the SIM6 callus, which lack regenerative capabilities[33]. Due to morphological similarities, we hypothesized that these cells may transcriptionally correspond to N4 at CIM7. Supporting this, *AT2G22510* and *PELPK1* were highly expressed in cluster 17 of the SIM6 cell atlas by Ogura *et al.*, which matched one of the "highly expanded globular cell" clusters (Supplementary Fig. S6i). Additionally, genes enriched in CIM7 cluster 13 were most highly expressed in cluster 17 of the SIM6 atlas (Supplementary Fig. S6i). Thus, N4 cells, marked by *AT2G22510* and *PELPK1*, represent "fully differentiated callus cells" that have lost their pluripotency (Fig. 2c). We therefore named this cell type as the "vacuolized cells".

N5 cells were predominantly located in the inner ACR and vascular tissues of explants and were characterized by genes linked to vascular development, such as *SMAX1-LIKE 3* (*SMXL3*), *XYLOGEN PROTEIN 2* (*XYP2*), *HOMEOBOX GENE 8* (*HB8*), and *ACL5* (Fig. 2b, c; Supplementary Figs. S4b and S7a). *ACL5* and *ABNORMAL SHOOT 5* (*ABS5*) reporters were initially expressed in the stele's procambium from CIM0 to CIM3 (Supplementary Fig. S7b, c). By CIM3, *ACL5* was ectopically expressed within the ACR, and *ABS5* expression was also detected in the ACR at CIM7. Although no anatomical features typical of vascular tissue, such as SE or TE formation, were observed in the ACR, *ACL5* and *ABS5*-positive cells exhibited a striped pattern resembling vascular organization (Fig. 2b; Supplementary Fig. S7b, c). These results indicate that N5 represents cells with vascular-like attributes; therefore, we assigned them as "vascular-like cells".

In summary, integrating time-resolved scRNA-seq and spatial transcriptomics revealed previously unrecognized spatial heterogeneity within callus tissues. Notably, callus organization can be categorized not only into outer, middle, and inner layers perpendicular to vascular bundles but also into FCR and ACR regions parallel to vascular bundles (Fig. 2c). In particular, the ACRs exhibit an organization resembling root primordium-like structures based on marker gene expression.

This heterogeneity likely results from asynchronous cell division patterns within explants. To test this hypothesis, we employed a constitutive nuclear localization reporter (*pAT2G18020:H2B-mCherry*)[61] to monitor the dynamics of cell layer formation in ACRs and FCRs. The results revealed that cell layer proliferation occurred more rapidly in ACRs than in FCRs (Fig. 2d; Supplementary Fig. S8a). Notably, the formation of two distinct cell layers in ACRs predominantly appeared at CIM2, whereas in FCRs, this process typically began at CIM4 (Fig. 2e; Supplementary Fig. S8a). These observations were further corroborated through live-cell imaging

using PlaCCI (Supplementary Fig. S8c, d; Supplementary Video S1)[62], which showed a higher frequency of G2–M reporter signals — indicative of active mitosis — in ACRs during CIM3 to CIM5.

To further assess the initiation of cell division in pericycle cells corresponding to ACRs and FCRs, we utilized Cytrap[63], a synthetic dual-color reporter that simultaneously visualizes the S-to-G2 and G2-to-M transitions of the cell cycle. At CIM1, approximately 87% of ACR regions had already initiated cell division, in contrast to only 28% of FCR regions (Fig. 2f; Supplementary Fig. S8b).

Together, these findings demonstrate that the differential formation of ACRs and FCRs arises from both the distinct onset timing of pericycle cell division and the varying proliferation rates of the resulting callus cells. These two factors collectively drive the more rapid development of ACRs, leading to a greater number of cell layers compared with FCRs.

Identification of ACRs as ineffective callus regions within the callus

The newly identified N2, N3, and N5 cells correspond to dome-shaped ACRs, traditionally considered effective callus areas capable of shoot formation during the SIM stage[32]. As such, we tracked ACR fate at CIM7 using wild type explants (Supplementary Fig. S9a–c) and *ACL5*, *YUC3*, and *ABCB15* reporters (Fig. 3a–c). Surprisingly, we found that these ACRs were committed into roots after transfer to the SIM. Specifically, *ACL5*-marked callus regions transitioned into vascular tissues of the root during the SIM stage (Fig. 3c), while *YUC3*- and *ABCB15*-marked callus regions differentiated into root cap cells (Fig. 3a, b).

A previous study demonstrated that lateral root meristems can be reprogrammed into shoot meristems in a specific timeframe through SIM[64], prompting us to examine whether ACRs retain residual plasticity to transition into shoots during *de novo* shoot organogenesis (DNSO). To address this, we performed a more refined, long-term cell fate tracking experiment from SIM0 to SIM17 using the *ACL5* reporter line and spinning disk confocal microscopy (Fig. 3d; Supplementary Fig. S9d, e), which reduced imaging time and phototoxicity. The ACL5^{+} callus regions were those exhibiting a striped expression pattern of *ACL5* (Supplementary Fig. S7b). As shown in Fig. 3e, only 2.1% of *ACL5*-labeled ACRs developed into shoots (n = 10/471), while 88.3% developed into roots, consistent with earlier tracking results (Fig. 3a–c; Supplementary Fig. S9a–c). By contrast, simultaneously tracking of the FCRs (i.e., non-ACL5-labeled regions) revealed that FCRs either developed into shoots or retain their original cell fate (Supplementary Fig. S10a–e).

Collectively, these findings indicate that not all callus regions possess pluripotency for shoot regeneration. Contrary to prior assumptions, the majority of multilayered ACRs fail to form shoots and do not transition into shoot meristems under SIM conditions (Fig. 3f). Nevertheless, ACRs retain limited cell fate plasticity, similar to lateral root meristems[64], exhibiting a rare capacity for shoot conversion within a transient developmental window (Fig. 3e).

As outlined above, callus development and ACR formation occur asynchronously. Would transferring calli earlier than CIM7 — before extensive ACR formation — enhance shoot regeneration? To address this, we performed a time-course experiment, transferring calli cultured on the CIM for varying durations to the SIM to evaluate their shoot regeneration potential (Supplementary Fig. S11a). Our results showed that calli earlier than CIM4 lacked shoot regeneration capacity, while those at CIM5 and CIM6 exhibited shoot regeneration rates comparable to CIM7.

These findings indicate that a minimum of four days is required for some callus cells to complete reprogramming and acquire pluripotency. Such prolonged culture time necessary for pluripotency acquisition inevitably lead to ACR formation, reflecting an unresolved conflict between asynchronous callus development and the extended time required to acquire pluripotency. Interestingly, epigenetic profiling results indicate that most ACRs may have adopted a root-like identity while simultaneously losing the open chromatin configuration required for shoot regeneration (Supplementary Text S1 and Fig. S11b–n). Notably, a long-term cell fate tracking experiment revealed that FCRs are likely not an early developmental state of ACRs (Supplementary Text S1 and Fig. S10d, e). Thus, the above results indicate that shoot regeneration competence is only restricted to discrete cellular states within *Arabidopsis* callus.

Chemical screening identifies compounds to reduce ineffective callus regions

Our findings indicate that ACRs represent ineffective callus regions that preferentially develop into roots on the SIM. Interestingly, we observed a strong negative correlation between the number of roots and shoots formed (Fig. 4a, b). Plants with higher shoot numbers tended to form fewer roots, whereas those with fewer shoots exhibited greater root development. Moreover, root numbers significantly exceeded shoot numbers (Supplementary Fig. S12a), suggesting that reducing the proportion of ACRs within callus tissues could enhance shoot regeneration efficiency. Inspired by advances in chemically induced pluripotent cells in animal research[65], we sought to identify compounds that could effectively diminish ACR proportions through chemical screening.

To establish a high-throughput screening system, we leveraged marker genes associated with ineffective callus regions. As noted, *ACL5* expression predominates in ACRs (Fig. 3c). We hypothesized that *ACL5* reporter fluorescence intensities could serve as a rapid proxy for assessing compound efficacy, circumventing the need to measure shoot regeneration efficiency directly and improving time use. To facilitate compound application and limit the costs of compounds, we developed a 24-well liquid culture system for calli (Fig. 4c). In this setup, groups of eight explants were cultured per well with liquid CIM supplemented with specific compounds. Preliminary tests confirmed that calli regenerated normally from hypocotyl explants after seven days under liquid CIM conditions in the absence of chemical treatment (Supplementary Fig. S12b). Expression patterns of reporters like *WOX5*, *PLT1*, and *ATML1* remained unchanged (Supplementary Fig. S12c).

We screened 92 compounds from a chemical library targeting factors involved in signal transduction (Supplementary Fig. S12d and Table S1). In the first round, while most compounds did not alter ACL5 reporter fluorescence, 27 compounds

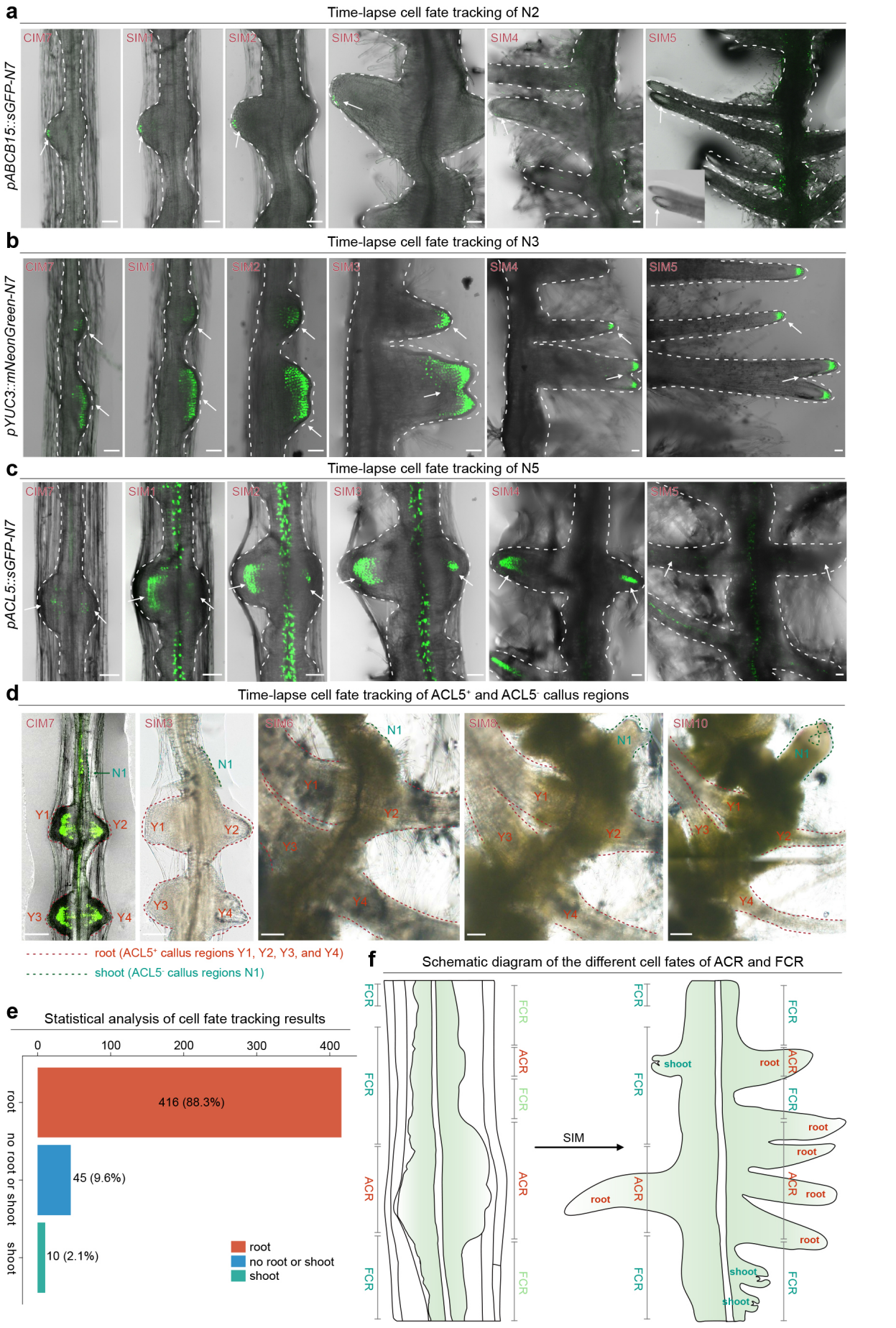

a
Time-lapse cell fate tracking of N2
pABCB15::sGFP-N7
CIM7
SIM1
SIM2
SIM3
SIM4
SIM5
b
Time-lapse cell fate tracking of N3
pYUC3::mNeonGreen-N7
c
Time-lapse cell fate tracking of N5
pACL5::sGFP-N7
d
Time-lapse cell fate tracking of ACL5+ and ACL5- callus regions
SIM6
SIM8
SIM10
N1
Y1
Y2
Y3
Y4
root (ACL5+ callus regions Y1, Y2, Y3, and Y4)
shoot (ACL5- callus regions N1)
e
Statistical analysis of cell fate tracking results
0
100
200
300
400
416 (88.3%)
45 (9.6%)
10 (2.1%)
root
no root or shoot
shoot
f
Schematic diagram of the different cell fates of ACR and FCR
FCR
ACR
SIM
shoot
root

Fig. 3 Identification of ACRs as ineffective callus areas within the callus. a–c Time-lapse cell fate tracking of N2 (**a**), N3 (**b**), and N5 (**c**) using specific fluorescence reporters driven by the regulatory sequences of *ABCB15* (**a**), *YUC3* (**b**), and *ACL5* (**c**), respectively. The callus outlines are marked with dashed lines. Representative calli for each reporter are shown. Calli at CIM7 were transferred to the SIM, and expression patterns were tracked daily from CIM7 to SIM5. The white arrows represent the tracked callus regions. Please note that the *ACL5* reporter was consistently active in the original vascular tissues of the explants (**c**). Scale bars, 50 µm. **d** Time-lapse cell fate tracking of $ACL5^+$ and $ACL5^-$ regions. Representative images of calli are shown, with N1 denoting $ACL5^-$ regions and Y1–Y4 indicating $ACL5^+$ regions. *ACL5* is constantly expressed in the vascular tissues of the explant. Therefore, the $ACL5^+$ callus regions are those exhibiting a striped expression pattern of *ACL5* (Supplementary Fig. S7b). Regions that developed into roots and shoots are outlined by red and green dashed lines, respectively. Calli were imaged every 2–4 days from CIM7 to SIM17. Data from SIM10 to SIM17 are not shown, as the cell fates of N1 and Y1–Y4 were already determined by that point. Scale bars, 100 µm. **e** Statistical summary of cell fate tracking results. Data are from three independent experiments. In total, 471 $ACL5^+$ regions from 16 explants were tracked, and the final fates of ACRs were classified into three categories: root, no root or shoot, and shoot. The percentage distribution of each category is shown. Notably, only 2.1% of ACRs developed into shoots. **f** Schematic diagram of the different cell fates of ACR and FCR. On the left, the entire callus at CIM7 is divided into two regions: ACR and FCR. Upon transfer to the SIM, the majority of ACRs developed into roots, representing ineffective callus regions, while shoots tended to derive from cells in the FCR. See also Supplementary Fig. S9.

significantly reduced reporter activity while incompletely blocking callus proliferation (Fig. 4d; Supplementary Fig. S12e, f). Validation in a second round identified eight candidate compounds (Fig. 4c, f), from which six were selected for further analysis, including assessments of their effects on shoot regeneration.

Consistent with the results of the liquid culture, candidate compounds significantly reduced $ACL5^+$ cell populations in calli cultured on the CIM compared to DMSO controls (Fig. 4d). However, while all compounds reduced root formation, not all enhanced shoot regeneration (Fig. 4d–f). For instance, Pemetrexed and Vismodegib did not improve shoot regeneration. Conversely, Ki8751, Patupilone, and CYC116 significantly reduced shoot regeneration capacity, with patupilone severely impairing callus proliferation. Among the tested compounds, U0126-EtOH was the sole compound that significantly enhanced shoot regeneration efficiency.

U0126 enhances shoot regeneration efficiency by reducing ineffective callus regions

The screened compound U0126-EtOH contains ethanol molecules. To rule out ethanol's influence on shoot regeneration, we compared the effects of U0126-EtOH and U0126 (ethanol-free). Both forms actually exhibited equivalent efficacy in inhibiting root development and promoting shoot regeneration (Supplementary Fig. S12g, h). To determine the optimal concentration of U0126, we tested concentrations ranging from 0.5 to 50 µM on the CIM and evaluated shoot regeneration on the SIM (Fig. 5a, b). Results showed peak shoot regeneration at 5 µM, with higher concentrations offering no significant improvement. Thus, 5 µM was chosen as the optimal concentration for subsequent phenotypic and mechanistic studies.

We then sought to investigate the reason why U0126 significantly enhances shoot regeneration efficiency. As shown in Fig. 5c, d, U0126-treated calli exhibited reduced fluorescence signals of the *ACL5* reporter and fewer cell layers. These findings suggest that U0126 effectively minimizes ineffective callus regions. Additionally, U0126 treatment substantially reduced $YUC3^+$ and $ABCB15^+$ cell populations in calli (Fig. 5c, d), indicating a broad reduction of ineffective regions rather than specific inhibition of *ACL5* expression.

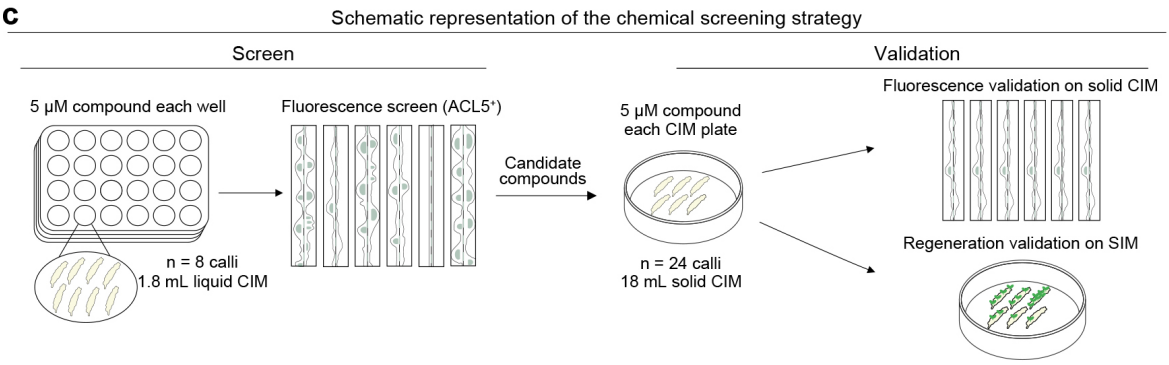
Using the PlaCCI system combined with cell layer tracking, we compared cell division dynamics between mock-treated and U0126-treated explants. U0126 treatment markedly reduced the division rate of callus cells (Fig. 5f–h; Supplementary Fig. S13a and Videos S2 and S3). Because ACR cells divide earlier and more rapidly than FCR cells (Fig. 2d–f; Supplementary Fig. S8), the inhibitory effect of U0126 was more pronounced in ACRs. Detailed analyses of cell cycle phase reporters and 5-ethynyl-2'-deoxyuridine (EdU) incorporation revealed that U0126 primarily induced cell cycle arrest at the G1–S checkpoint or within the S phase by reducing DNA synthesis (Fig. 5h; Supplementary Fig. S13a–c).

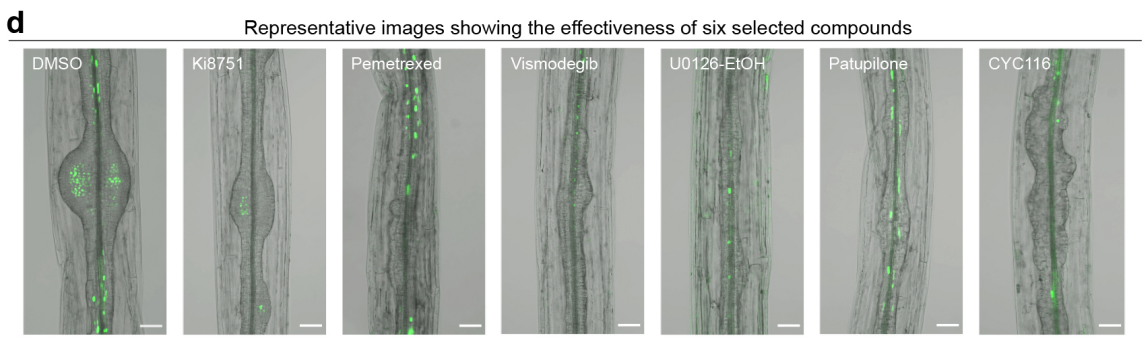
To determine whether U0126's function was solely due to suppressed cell division, we treated calli on CIM with flavopiridol (FVP) and hydroxyurea (HU) — which inhibit cell cycle progression at the G1–S and G2–M phases[56,61], and nocodazole (NOCO), a cyclin inhibitor that blocks the G2-M transition in *A. thaliana* callus[56,66]. Unlike U0126, FVP, and HU, NOCO was cytotoxic, causing abnormal cell morphology (Supplementary Fig. S13d). Although FVP and HU exhibit a stronger capacity to inhibit cell division than U0126 (Supplementary Figs. S13e, f), they only modestly enhanced shoot regeneration efficiency (Supplementary Fig. S13g).

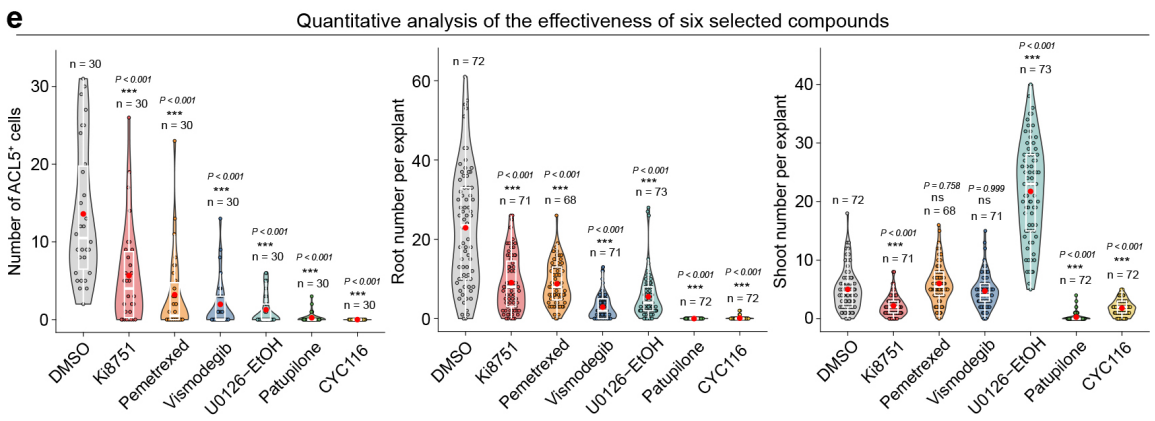
Previous studies suggest that middle-layer formation in callus tissue is crucial for pluripotency and shoot formation[32]. Mutants of middle-layer genes, such as *WOX5*, *WOX7*, *PLT1*, and *PLT2*, exhibit reduced shoot regeneration capacity[29,32,56]. However, U0126 treatment did not significantly alter the expression patterns of *WOX5* or *PLT1* reporters in calli at CIM7 (Fig. 5e; Supplementary Fig. S14a). Similarly, the expression of outer-layer gene reporters, such as *ATML1* and *KCS10*, remained unchanged (Fig. 5e; Supplementary Fig. S13h). Thus, U0126 does not appear to enhance shoot regeneration by directly influencing pluripotency genes on the CIM.

To further investigate U0126's effects, we cultured wild-type explants on the CIM with U0126 or DMSO (control) and conducted RNA-seq on calli at CIM7 and SIM6 (the stage of SAM commitment). At CIM7, U0126-treated calli exhibited upregulated expression of genes involved in immune response, stress response, toxin metabolism, and endoplasmic reticulum-associated protein degradation pathways (Supplementary Fig. S14a–c). Downregulated genes were linked to mitosis, cell wall synthesis, root and vascular development, and auxin synthesis and transport (Supplementary Fig. S14a–f). At SIM6, U0126-treated calli showed increased expression of SAM-related genes, including *WUS*, *CLAVATA3* (*CLV3*), and *SHOOT MERISTEMLESS* (*STM*), while genes associated with vascular development and transport, such as


a
The inverse correlation between the number of regenerated shoots and roots
root
shoot
b
Scatter plot of root and shoot numbers
R = -0.36, P = 1.3 e-07
Root number per explant
Shoot number per explant


c
Schematic representation of the chemical screening strategy
Screen
Validation
5 μM compound each well
Fluorescence screen (ACL5+)
Candidate compounds
5 μM compound each CIM plate
Fluorescence validation on solid CIM
Regeneration validation on SIM
n = 8 calli
1.8 mL liquid CIM
n = 24 calli
18 mL solid CIM


d
Representative images showing the effectiveness of six selected compounds
DMSO
Ki8751
Pemetrexed
Vismodegib
U0126-EtOH
Patupilone
CYC116


e
Quantitative analysis of the effectiveness of six selected compounds
Number of ACL5+ cells
Root number per explant
Shoot number per explant
DMSO
Ki8751
Pemetrexed
Vismodegib
U0126-EtOH
Patupilone
CYC116

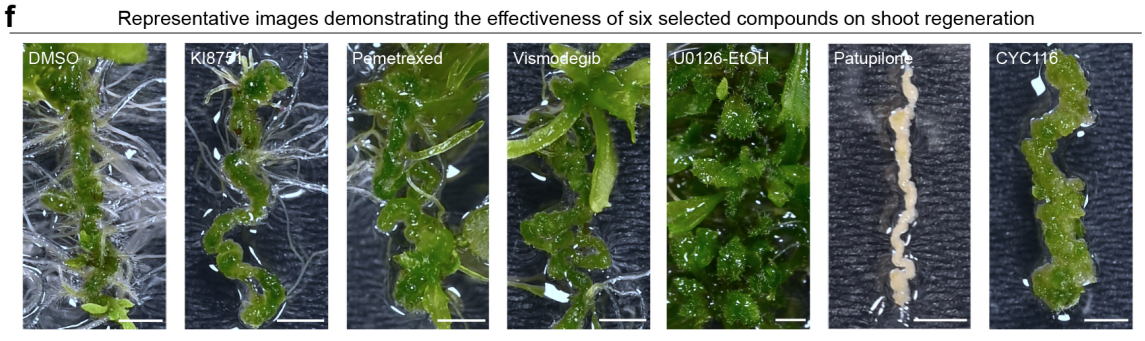

f
Representative images demonstrating the effectiveness of six selected compounds on shoot regeneration
DMSO
Ki8751
Pemetrexed
Vismodegib
U0126-EtOH
Patupilone
CYC116

Fig. 4 Chemical screening identifies candidate compounds reducing ineffective callus regions. a Representative images illustrating an inverse correlation between the number of regenerated shoots and roots. Hypocotyls from 7-day-old wild-type seedlings grown in the dark were used as explants. After culturing on CIM for 7 days, calli were transferred to the SIM, and regeneration phenotypes were assessed at SIM16. Note that calli with more roots typically produced fewer regenerated shoots, and *vice versa*. Scale bars, 2 mm. **b** Scatter plot illustrating the inverse correlation between the number of regenerated shoots and roots, with a univariate linear regression fitting curve applied. Data are from three independent experiments. A total of 198 callus explants were analyzed. **c** Schematic representation of the chemical screening strategy. *ACL5* reporter, which marks the ACRs, was used for detection. Eight calli were cultured in each well, with 1.8 mL of liquid CIM. The effectiveness of compounds was assessed by the number of fluorescence foci (i.e., $ACL5^+$ cells). Candidate compounds identified in the initial screening were validated based on $ACL5^+$ cell counts and shoot regeneration phenotypes. **d** Representative images showing the effectiveness of six selected compounds. $ACL5^+$ cells are shown in green. DMSO served as the control. Scale bars, 50 μm. **e** Quantitative analysis of the effectiveness of six selected compounds. The number of $ACL5^+$ cells (left), regenerated roots (middle), and regenerated shoots (right) were quantified. The regeneration protocol was the same as in **a**. Data were assessed at SIM16 and visualized as violin plots. The number of callus explants is indicated above each column. Data are from one representative experiment of three independent experiments. Medians (middle bar), quartiles (boxes), and 1.5× interquartile ranges (whiskers) are shown. Red dots represent means. Statistical analysis was performed using one-way ANOVA with Tukey's multiple comparisons. $^{***}P < 0.001$; ns, no significant difference. **f** Representative images demonstrating the effectiveness of six selected compounds on shoot regeneration. Scale bars, 2 mm. See also Supplementary Fig. S12.

SWEET11 and *UMAMIT20*, were downregulated (Supplementary Fig. S14d).

Finally, to test whether U0126 enhances shoot regeneration by accelerating the emergence of WUS^+ cells on the SIM, we used the *pWUS::DsRed-N7* reporter line[67]. Calli cultured on the CIM with U0126 and transferred to the SIM did not exhibit earlier WUS^+ cell appearance compared to controls (Supplementary Fig. S14g). Taken together, these findings indicate that U0126 reduces the level of ineffective callus regions by synchronizing callus growth and limiting root-like characteristics within ACRs (Fig. 6h; Supplementary Fig. S14a, c, d).

U0126 reduces ineffective callus regions via the MKK4/5–MPK3/6 pathway

Based on compound annotation and prior plant studies[68,69], U0126 is an inhibitor of MAPK kinases (MPKKs, also known as MEKs) that phosphorylate mitogen-activated protein kinases (MPKs)[70]. Its effects are unlikely to reflect off-target activity, as additional MEK inhibitors elicited comparable, though weaker, enhancements in shoot regeneration (Supplementary Fig. S15). In *A. thaliana*, 10 MPKKs are classified into four groups based on sequence similarity[71]. Two key MPKK–MPK signaling cascades with distinct roles in plant development have been identified: (1) the MKK4/5–MPK3/6 pathway, which regulates processes such as stomatal development, floral organ abscission, lateral root emergence, hormone response, hypoxia signaling, and immunity[72–74]; and (2) the MKK1/2–MPK4 cascade, which is associated with plant immunity, cold responses, and aluminum resistance[75].

Comparative studies revealed that the *mkk1/2* double mutants exhibited lower shoot regeneration efficiency compared to the wild-type (Supplementary Fig. S16c). Since the *mkk4/5* double mutants are lethal, conditional *mkk4/5* mutants (*mkk4,5RNAi-est*) were used[73]. Silencing *MKK4/5* via estradiol (ES) treatment resulted in slender calli resembling those treated with U0126 (Fig. 6a, b; Supplementary Fig. S16a, b). These calli displayed increased shoot regeneration efficiency, reduced root formation (Fig. 6c), fewer ineffective callus protrusions, and diminished fluorescence intensities of the ACL5 reporter (Fig. 6d, e). GO and PO enrichment analyses demonstrated substantial overlap in gene expression changes between U0126-treated and *mkk4,5RNAi-est* calli (Supplementary Figs. S14b, c, and S16d–i), indicating that U0126 primarily functions through the MKK4/5 pathway.

To validate these findings, we performed scRNA-seq on *mkk4,5RNAi-est* calli at CIM7. ES-treated calli exhibited reduced cell heterogeneity, indicative of synchronized growth (Fig. 6f; Supplementary Fig. S16j). Integration analyses revealed a lower proportion of callus cells (clusters 2 and 5) (Supplementary Fig. S16k), enriched in vascular tissue-related genes such as *ACL5* and *SMXL3* (Supplementary Fig. S16l).

MPK3/6 serves as the principal downstream target of MKK4/5[72–74,76]. We therefore examined whether *mpk3/6* mutants display regeneration phenotypes similar to *mkk4,5RNAi-est* plants. As homozygous *mpk3/6* double mutants are lethal, we utilized the conditional mutant line *MPK3SR*[72]. Consistent with expectations, silencing *MPK3/6* resulted in the formation of slender calli exhibiting enhanced shoot regeneration efficiency and reduced root formation (Supplementary Fig. S16m), closely resembling the phenotype induced by U0126 treatment. Notably, U0126 treatment did not further enhance the shoot regeneration efficiency of *MPK3SR* and *mkk4,5RNAi-est* explants (Fig. 6g), indicating that the MKK4/5-MPK3/6 cascade is likely the primary target through which U0126 exerts its effects.

It is worth noting that *MKK4/5* and *MPK3/6* show no tissue or cellular specificity within the callus (Supplementary Fig. S14h). Differential phosphoproteomic analysis further revealed substantial decreases in the phosphorylation of proteins implicated in epigenetic regulation, the cell cycle, and auxin transport following U0126 treatment (Supplementary Text S1 and Fig. S17).

Collectively, these results demonstrate that U0126 suppresses the formation of ineffective callus regions through an MKK4/5–MPK3/6-associated pathway (Fig. 6h). In agreement with the transcriptomic and scRNA-seq data, U0126 likely acts through multiple MPK3/6 downstream targets — coordinating callus development not only by restricting cell division but also by regulating genes associated with auxin biosynthesis and transport, cell wall remodeling, and vascular tissue differentiation. Nonetheless, the specific MPK3/6 targets mediating these effects require further investigation.

U0126 promotes shoot regeneration in other species

To assess U0126's efficacy across species, we first tested it within the Brassicaceae family. In *Crucihimalaya wallichii*, a close relative of *A. thaliana* that has recently been used in studies on perennial life history[77], U0126 treatment during CIM induced slender calli similar to those in *A. thaliana*

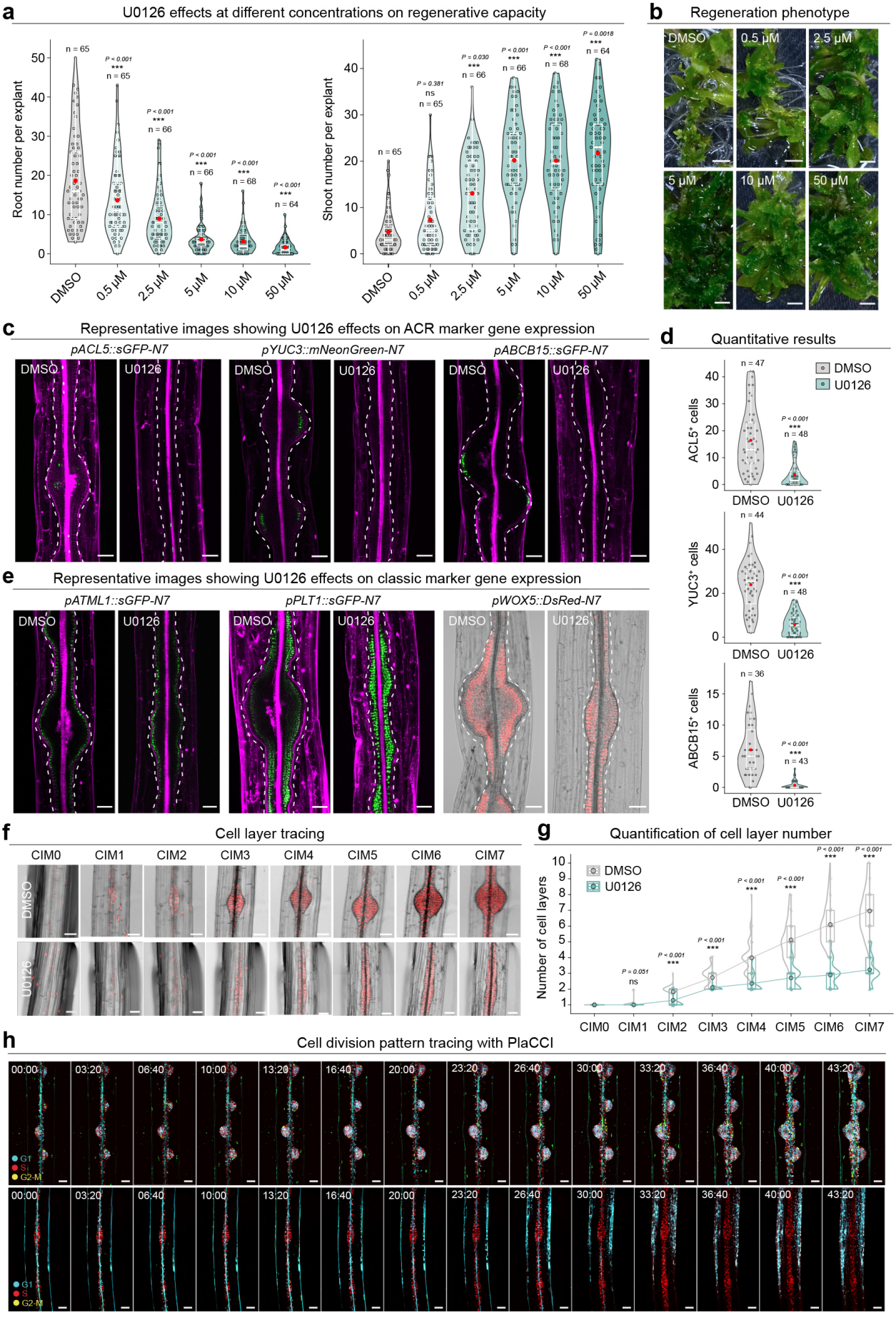

a
U0126 effects at different concentrations on regenerative capacity
Root number per explant
Shoot number per explant
DMSO
0.5 μM
2.5 μM
5 μM
10 μM
50 μM
b
Regeneration phenotype
c
Representative images showing U0126 effects on ACR marker gene expression
pACL5::sGFP-N7
pYUC3::mNeonGreen-N7
pABCB15::sGFP-N7
U0126
d
Quantitative results
ACL5+ cells
YUC3+ cells
ABCB15+ cells
e
Representative images showing U0126 effects on classic marker gene expression
pATML1::sGFP-N7
pPLT1::sGFP-N7
pWOX5::DsRed-N7
f
Cell layer tracing
CIM0
CIM1
CIM2
CIM3
CIM4
CIM5
CIM6
CIM7
g
Quantification of cell layer number
Number of cell layers
h
Cell division pattern tracing with PlaCCI
G1
S
G2-M

Fig. 5 Identification of U0126 as an effective compound to reduce ineffective callus regions. a Effects of U0126 at different concentrations on regeneration efficiency. The number of regenerated roots (left) and shoots (right) was quantified at SIM16 and displayed as violin plots. Callus explant counts are shown at the top of each column. Data are from one representative experiment of three independent experiments. Medians (middle bars), quartiles (boxes), and 1.5× interquartile ranges (whiskers) are indicated. Red dots represent Means. Statistical analysis was performed using one-way ANOVA with Tukey's multiple comparisons. ***$P < 0.001$; ns, no significant difference. **b** Representative images showing the impact of U0126 concentrations on regeneration efficiency. Scale bars, 2 mm. **c, e** Representative images showing the effects of U0126 on ACR (**c**) and other classic marker (**e**) gene expression. DMSO was used as a control. Images were taken at CIM7. Cell outlines were stained with propidium iodide (magenta). Scale bars, 50 µm. **d** Quantitative analysis of ACR marker gene expression under U0126 treatment. Numbers of $ACL5^+$, $YUC3^+$, and $ABCB15^+$ cells in calli at CIM7 were quantified. DMSO served as a control. Data are shown as violin plots with callus explant counts at the top of each column. Data are from one representative experiment of three independent experiments. Statistical significance was assessed using student *t*-test, ***$P < 0.001$. **f, g** Quantification of the rate of increase in cell layer number using a constitutive nuclear localization reporter (*pAT2G18020:H2B-mCherry*). Representative callus images and corresponding quantification results are shown in **f** and **g**, respectively. Mock- and U0126-treated callus regions were imaged daily from CIM0 to CIM7. Four explants treated with DMSO (mock) and three explants treated with U0126 were analyzed and quantified. *n* represents the number of tracked callus regions ($n = 89$ for mock and $n = 83$ for U0126-treated samples). Statistical analysis in **g** was performed using the Mann-Whitney test. ***$P <$ 0.001; ns, no significant difference. Scale bars in **f**, 50 µm. **h** Analysis of cell division dynamics in mock- (upper row) and U0126-treated (lower row) calli from CIM3 to CIM5 using live imaging with PlaCCI. A total of 66 imaging sessions were performed, each with 40-minute intervals. The three cell cycle phases (G1, S, and G2–M) are represented by distinct fluorescent signals. Compared to mock-treated samples, U0126 treatment resulted in a noticeable reduction of cyan fluorescence, corresponding to G1-phase cells. Non-nuclear cyan signals observed in the epidermal and cortex cells of U0126-treated samples were due to U0126 autofluorescence. Quantification is provided in Supplementary Fig. S13a. Scale bars, 50 µm.

(Supplementary Fig. S18a). These calli produced fewer roots and more shoots upon transfer to the SIM (Fig. 7a; Supplementary Fig. S18b), indicating U0126's broad applicability in the *Arabidopsis* clade. Next, we evaluated U0126 in the oil crop *Brassica napus*, testing two varieties with distinct life histories: ZS11 (semi-winter-type), and Tapidor (winter-type). As shown in Fig. 7b and Supplementary Fig. S18f, U0126 significantly enhanced shoot regeneration in both varieties.

To extend the applicability of our method beyond the Brassicaceae family, we conducted regeneration experiments on the plants from other families, including Solanaceae and Poaceae. Notably, we found that U0126 treatment during CIM could also significantly boost shoot regeneration efficiency in *Capsicum annuum* (Solanaceae) and *Setaria viridis* and *Oryza sativa* (Poaceae) (Fig. 7c–e).

It is important to recognize that plant species differ markedly in genotypes and developmental programs. Moreover, tissue culture-based regeneration is a multistep process, and defects during the SIM stage can further constrain regenerative capacity[11]. Accordingly, compounds such as U0126, which primarily reduce the proportion of ineffective callus regions during CIM, are unlikely to constitute a universal solution (Supplementary text S1 and Figs. S18–S20). Nevertheless, our results establish a four-step optimization framework that represents a substantial practical advance over traditional trial-and-error approaches, which typically focus on modifying medium composition or adjusting culture duration and temperature (Supplementary Fig. S21)[13]. This framework can be readily extended to large-scale compound screening across species or regeneration stages. In the near future, it may facilitate the identification of species- or family-specific compounds or cocktails (see Discussion below), ultimately alleviating persistent bottlenecks in plant regeneration.

DISCUSSION

Our findings indicated that high auxin concentrations in the CIM, along with rapid cell division in ACR, causes a swift cell reprogramming toward root identity and a loss of shoot regeneration potential. In contrast, FCR cells retain pluripotency, potentially due to fewer rounds of cell division, preventing them from reaching the epigenetic threshold required for root identity. U0126 treatment reduced cell division, synchronized callus development, and reduced ACR proportions. However, cell division alone is not the sole determinant of pluripotency. Simply inhibiting cell division does not guarantee that all callus cells acquire or maintain pluripotency (Supplementary Fig. S13e–g). These findings suggest a critical time window for pluripotency acquisition and are consistent with recent observations that stem cell activity is transiently acquired and subsequently lost in the callus[78]. Given that numerous studies have documented pronounced heterogeneity in the regenerative capacity of rice callus, with regeneration progressively declining during prolonged culture[14,15], it is highly plausible that similar principles apply to calli derived from other tissue sources. However, critical questions remain unresolved. For instance, do similar ineffective regions exist in calli derived from immature or mature embryos of monocots like rice, wheat, and maize? If so, what genes mark these regions?

The asynchrony in *A. thaliana* callus development also warrants further exploration. Could inherent differences in pericycle cell responsiveness to auxin signals explain this phenomenon? Are spatial variations in auxin concentration a contributing factor, or is this asynchrony purely stochastic? To date, long-term cell fate tracking has not revealed definitive patterns. Our findings suggest that U0126 functions through the MKK4/5–MPK3/6 signaling cascade, whose phosphorylation of multiple downstream targets (Fig. 6h), collectively slows cell division, synchronizes developmental progression, and preserves the pluripotent cell state required for efficient shoot regeneration. Interestingly, the MAPK pathway also regulates cell fate manipulation in animals[65,79], hinting at shared principles of cellular pluripotency or totipotency between plants and animals.

This study opens new research avenues akin to the field of stem cells in animals. Chemical reprogramming[65,80,81] may enable cell fate transitions, producing stem cells and diverse plant organs. Notably, other MEK inhibitors were less effective than U0126 (Supplementary Fig. S15). Future efforts could focus on developing more potent compound cocktails

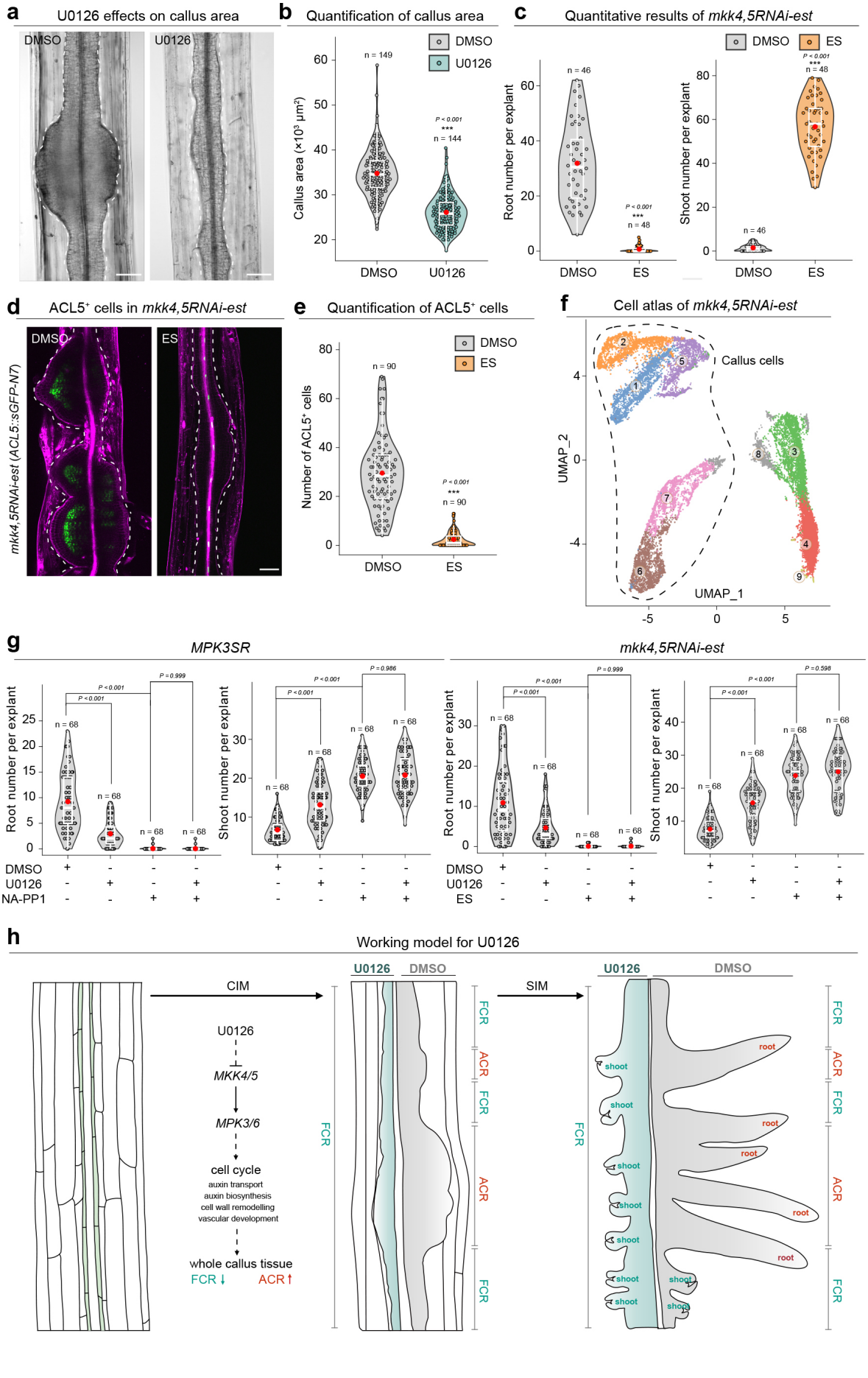

a
U0126 effects on callus area
DMSO
U0126
b
Quantification of callus area
DMSO
U0126
Callus area (×10³ μm²)
n = 149
n = 144
P < 0.001
***
DMSO
U0126
c
Quantitative results of mkk4,5RNAi-est
DMSO
ES
Root number per explant
Shoot number per explant
n = 46
n = 48
P < 0.001
***
d
ACL5⁺ cells in mkk4,5RNAi-est
mkk4,5RNAi-est (ACL5::sGFP-N7)
DMSO
ES
e
Quantification of ACL5⁺ cells
Number of ACL5⁺ cells
n = 90
P < 0.001
***
f
Cell atlas of mkk4,5RNAi-est
Callus cells
UMAP_1
UMAP_2
g
MPK3SR
mkk4,5RNAi-est
Root number per explant
Shoot number per explant
n = 68
P < 0.001
P = 0.999
P = 0.986
P = 0.598
DMSO
U0126
NA-PP1
ES
h
Working model for U0126
CIM
SIM
U0126
DMSO
MKK4/5
MPK3/6
cell cycle
auxin transport
auxin biosynthesis
cell wall remodelling
vascular development
whole callus tissue
FCR ↓
ACR ↑
FCR
ACR
shoot
root

Fig. 6 U0126 reduces ineffective callus regions through the MKK4/5–MPK3/6 pathway. a Representative images of U0126 effects on callus cell proliferation. Callus outlines are marked with dashed lines. Images were taken at CIM7. DMSO served as a control. Scale bars, 50 μm. **b** Quantitative analysis of callus area at CIM7 under U0126 treatment. Data are shown as violin plots with callus region counts at the top of each column. Data are from one representative experiment of three independent experiments. Medians (middle bars), quartiles (boxes), and 1.5× interquartile ranges (whiskers) are indicated. Red dots represent means. **c** Quantitative analysis of shoot and root regeneration phenotypes in *mkk4,5RNAi-est* calli. *MKK4/5* were silenced using RNAi under ES treatment. Calli were treated with DMSO (control) or 10 μM ES on the CIM, and phenotypes were measured at SIM16. Data are shown as violin plots with callus explant counts at the top of each column. Data are from one representative experiment of three independent experiments. **d** Representative images of *ACL5* expression in *mkk4,5RNAi-est* calli treated with ES on the CIM. Images were taken at CIM7. Dashed lines mark callus outlines. DMSO served as a control. Cell outlines were stained with propidium iodide (magenta). Scale bars, 50 μm. **e** Quantitative analysis of $ACL5^{+}$ cells in *mkk4,5RNAi-est* calli. Data are shown as violin plots with callus explant counts at the top of each column. Data are from one representative experiment of three independent experiments. **f** UMAP visualization of cell atlas in ES-treated *mkk4,5RNAi-est* calli at CIM7. Explants were cultured on CIM with DMSO (control) or 10 μM ES, and calli were harvested at CIM7 for scRNA-seq. Clusters corresponding to callus cells are outlined with dashed lines. Biological replicates: $n = 3$ for DMSO and $n = 2$ for ES. **g** Quantitative analysis of the effect of U0126 on shoot and root regeneration efficiency of *MPK3SR* and *mkk4,5RNAi-est* calli. *MPK3/6* and *MKK4/5* were silenced by treatment of NA-PP1 or ES respectively. Calli were treated with DMSO (control), 5 μM U0126, 0.5 μM ES or 10 μM ES were applied on the CIM, and regeneration phenotypes were measured at SIM19. Data are shown as violin plots with callus explant counts at the top of each column. Data are from one representative experiment of three independent experiments. Medians (middle bars), quartiles (boxes), and 1.5× interquartile ranges (whiskers) are indicated. Red dots represent Means. **h** Working model for U0126. U0126 reduces ACRs by inhibiting MKK4/5–MPK3/6 activity. Downstream targets are involved in processes such as the cell cycle, auxin biosynthesis and transport, cell wall remodeling, root cap development, and vascular development. Middle and right panels: U0126-treated callus (left) vs DMSO control (right). U0126 treatment flattens callus morphology, reduces ACRs, and increases FCRs, leading to more regenerated shoots on the SIM. In contrast, the DMSO control shows abundant ACRs, resulting in more roots and fewer shoots on the SIM. Statistical analyses were performed using a Student's *t*-test in **b**, **c**, **e** or one-way ANOVA with Tukey's multiple comparisons in **g**. $^{***}P < 0.001$. See also Supplementary Figs. S14, S16, and S17.

to further enhance regeneration efficiency. Indeed, epigenetic inhibitors have shown promise in improving plant regeneration capabilities[82-86]. Additionally, recent studies report that small molecules like adenosine monophosphate enhance *A. thaliana* regeneration competence, while plant peptides promote regeneration across species[87,88]. High-throughput chemical screenings in crops remain challenging but achievable. Identifying marker genes for effective and ineffective callus regions using single-cell multi-omics, spatial transcriptomics, and cell fate tracking will be crucial. Such markers will facilitate compound candidate screening via platforms similar to those described here, ultimately advancing plant tissue culture and regeneration technologies.

MATERIALS AND METHODS

Plant materials and growth conditions

The *Arabidopsis thaliana* (L.) *Heynh.* plants were used as the experimental model in the study. Columbia-0 (Col-0) ecotype was used as wild type with transgenic lines in this background. The Cytrap, PlaCCI, *pAT2G18020:H2B-mCherry*, *MPK3SR*, *mkk1/2* mutants, *pWUS::DsRed-N7*, and *mkk4,5RNAi*-est lines were described[61-63,67,72,73,75]. We crossed *mkk4,5RNAi*-est plant with *pACL5::sGFP-N7* plant to obtain *mkk4,5RNAi*-est *pACL5::sGFP-N7* line. The seeds for DNSO assays including *C. wallichii*, *S. lycopersicum* varieties, *B. napus* varieties, *S. viridis* ME034V, *C. annuum* CM334, *Oryza sativa* ZH11, and *M. sativa* Zhongmu No.1 were either maintained in our lab[77] or obtained from other labs.

Wild type plants were grown in growth room at 21 °C under long-day (16-h light/8-h dark) conditions. The calli were grown in Percival or RUIHUA incubators at specified temperatures under long-day or dark (wrapped in aluminum foil) conditions.

Generation of transgenic plants

To construct the fluorescent reporter lines that mimic the endogenous expression pattern, we defined the necessary upstream and downstream sequences of each cell-cluster enriched gene based on their local chromatin accessibilities. Details regarding the lengths of the upstream and downstream sequences for each gene, along with the primers used for vector construction, are provided in Supplementary Table S1.

The overall procedure involves amplifying the fragments using a high-fidelity enzyme and inserting the upstream and downstream DNA sequences of the gene into the binary vector via homologous recombination. Fragment amplification was carried out using 2× Phanta® Max Master Mix (Vazyme Biotech, Cat No./ID: P515-02). Fragment recovery was conducted using the FastPure Gel DNA Extraction Mini Kit (Vazyme Biotech, Cat No./ID: DC301-01). The recombination reactions were performed using the ClonExpress® MultiS One Step Cloning Kit (Vazyme, Cat No./ID: C113-02) or the ClonExpress® II One Step Cloning Kit (Vazyme, Cat No./ID: C112-02). For plasmid extraction, we used the High Purity Plasmid Mini Kit (Hlingene, Cat No./ID: NG201S).

The resultant binary constructs were then introduced into *Agrobacterium tumefaciens* GV3101 (pMP90) by the freeze-thaw method. Transgenic Arabidopsis plants were generated by the floral dipping method[89] and screened with 0.05% glufosinate (Basta) on soil, or 50 mg/L kanamycin on the half-strength Murashige and Skoog (1/2 MS) agar plates.

Shoot regeneration assays for *Arabidopsis thaliana* and *Crucihimalaya wallichii*

Shoot regeneration assays of *A. thaliana* and *C. wallichii* were performed as described previously[38,90]. Briefly, seeds were sterilized using 20% bleach and germinated on the 1/2 MS agar plate in the dark. After 7 days, 1 cm long hypocotyls of seedlings were excised, placed on the CIM, and cultured in a Percival incubator at 22 °C under long-day conditions with a light intensity of 45 μmol $m^{-2}·s^{-1}$. For *A. thaliana*, the hypocotyls were cultured on the CIM for 7 days, while for *C. wallichii*, the duration was extended to 14 days. The resultant calli were transferred to the SIM and cultured in a Percival incubator at 22 °C under long-day conditions with a light

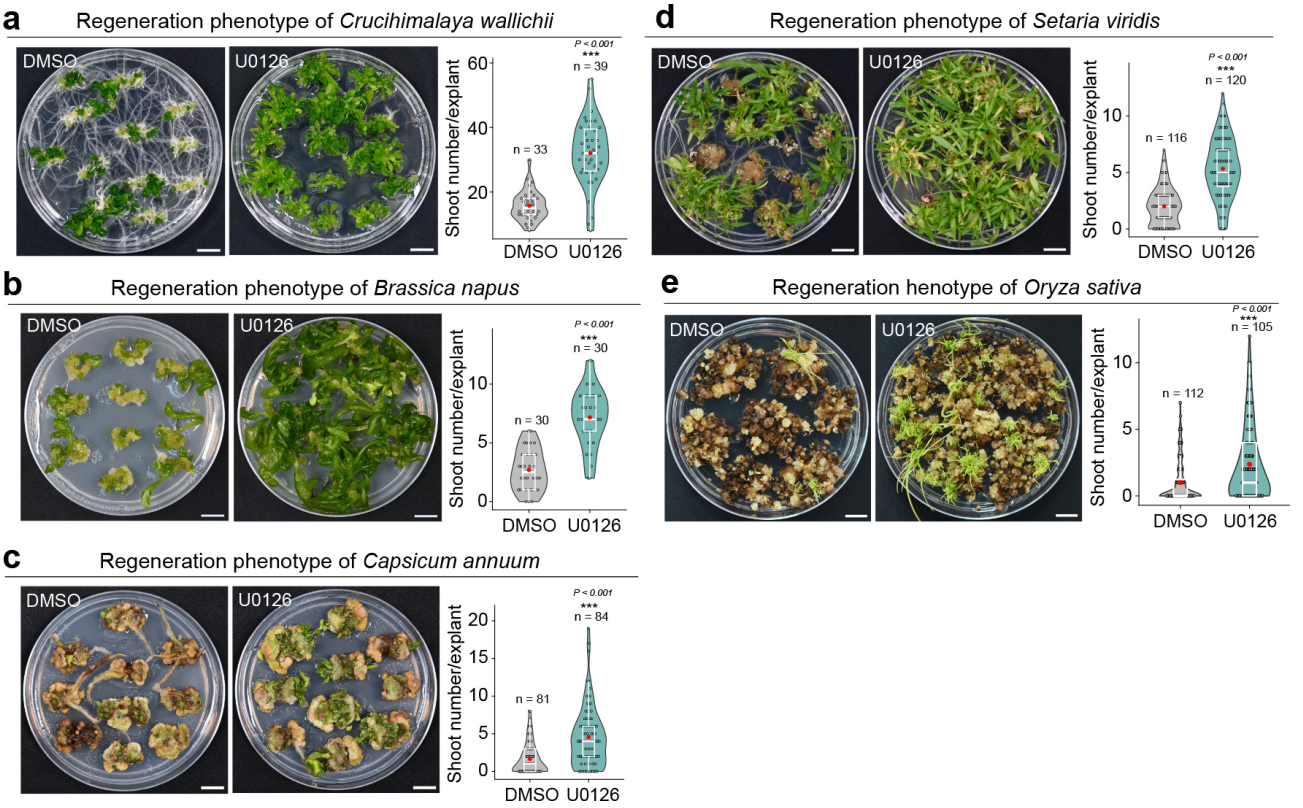


Fig. 7 Effect of U0126 on shoot regeneration efficiency across other species. a–e Impact of U0126 on shoot regeneration in *C. wallichii* (**a**), *B. napus* (**b**, ZS11), *C. annuum* (**c**), *S. viridis* (**d**), and *O. sativa* (**e**). Representative images (left) show the effect of U0126 on shoot regeneration. U0126 was applied at 50 μM for *B. napus* (ZS11); 20 μM for *O. sativa*; 10 μM for *C. annuum*; and 5 μM for *S. viridis*. Quantification dates: *C. wallichii* (SIM29) in **a**; *B. napus* (SIM29) in **b**; *C. annuum* (SIM34) in **c**; *S. viridis* (SIM50) in **d**; and *O. sativa* (SIM53) in **e**. The data on the right are shown as violin plots, with the number of callus explants indicated at the top of each column. Data are from one representative experiment of three independent experiments. Statistical analysis was performed using Student *t*-test. ***$P < 0.001$; **$P < 0.01$; *$P < 0.05$; ns, not significant. Scale bars, 1.0 cm. See also Supplementary Figs. S18–S20.

intensity of 80 μmol m^{-2}·s^{-1}. U0126 was only applied during the CIM stage.

The formulation of the 1/2 MS agar medium is as follows: 2.21 g MS basal medium w/vitamins powder (PhytoTech, Cat No./ID: M519-100L), and 8 g/L agar (Sangon Biotech, Cat No./ID: A505255-0250), pH 5.8. The formulation of CIM is as follows: 4.43 g MS basal medium w/vitamins powder (PhytoTech, Cat No./ID: M519-100L), 20 g/L sucrose (Abcone, Cat No./ID: S48029-1KG), 2.2 μM 2,4-dicholorophenoxyacetic acid (PhytoTech, Cat No./ID: D295-100mL), 0.2 μM kinetin (Sigma, Cat No./ID: 48130-1G-F), and 7 g/L agar (Duchefa, Cat No./ID: P1001.0500), pH 5.7. The formulation of SIM is as follows: 4.43 g MS basal medium w/vitamins powder (PhytoTech, Cat No./ID: M519-100L), 20 g/L sucrose (Abcone, Cat No./ID: S48029-1KG), 0.9 μM indole-3-acetic acid (Sigma, Cat No./ID: 45533), 5 μM 2-isopentenyladenine (Sigma, Cat No./ID: D7674), and 1.8 g/L phytagel (Sigma, Cat No./ID: P8169-250G), pH 5.8.

For chemical treatment in *A. thaliana*, candidate compounds and cell cycle inhibitors (such as FVP, HU, and NOCO) and inducers (such as ES and NA-PP1) are directly added to CIM before it solidifies. The hypocotyl explants were cultured on CIM containing the corresponding compounds or inhibitors for 7 days. The resulting calli were either phenotyped or further transferred to SIM without compounds or inhibitors to assess the efficiency of shoot regeneration. The concentrations used are specified in the figure legends.

Shoot regeneration assays for *Brassica napus*

The shoot regeneration assays for *B. napus* were performed as described previously, with some modifications[91]. The seeds were first washed with 75% ethanol for 1 min, then rinsed with sterile water for 5 times. The seeds were then washed with a 10% sodium hypochlorite solution (2 drops of Tween-20 per 50 mL) for 10 min, followed by 5 times of rinsing with sterile water, and placed in the dark at 4 °C. After 1 day, seeds were sown on the 1/2 MS agar plate and cultured in an RUIHUA incubator at 26 °C in the dark for 6–8 days. The hypocotyls of the seedlings were excised to a fixed length of approximately 1.5 cm and cultured on the CIM in a RUIHUA incubator at 26 °C in the dark for 21 days. If *n*-hexane (Macklin, Cat No./ID: H811147) treatment is required, the excised hypocotyls were placed on a dish containing *n*-hexane for 1 min and then transferred to the CIM. If squeezing treatment is required, the excised hypocotyls were placed on a petri dish, squeezed by ophthalmic tweezers, and then cultured on the CIM. To induce shoot regeneration, the resultant calli were transferred onto the SIM and cultured in a Percival incubator at 26 °C under long-day conditions with a light intensity of 80 μmol m^{-2}·s^{-1}. If the varieties ZS11 and Tapidor were used, the SIM was refreshed approximately every 14 days. If the variety Westar was used, no refreshment is necessary.

U0126 was only applied during the CIM stage.

The formulation of the 1/2 MS agar medium is the same as that for *A. thaliana*. The formulation of CIM is as follows: 4.43 g MS basal medium w/vitamins powder (PhytoTech, Cat No./ID: M519-100L), 30 g/L sucrose (Abcone, Cat No./ID: S48029-1KG), 18 g/L mannitol (Sigma, Cat No./ID: M4125-500G), 1 mg/L 2,4-dicholorophenoxyacetic acid (PhytoTech, Cat No./ID: D295-100mL), 0.3 mg/L kinetin (PhytoTech, Cat No./ID: K483-100mL), 1:10000 ratio STS (0.1 M $Na_2S_2O_3$:0.1 M $AgNO_3$ = 4:1), and 7 g/L agar (Duchefa, Cat No./ID: P1001.0500), pH 5.8. The formulation of SIM is as follows: 4.43 g MS basal medium w/vitamins powder (PhytoTech, Cat No./ID: M519-100L), 10 g/L glucose (Sigma, Cat No./ID: G7528-1KG), 0.25 g/L xylose (Sinopharm Chemical Reagent, Cat No./ID: 63012037), 0.6 g/L MES (Abcone, Cat No./ID: M38689-500G), 0.1 mg/L indole-3-acetic acid (PhytoTech, Cat No./ID: I364-100mL), 2 mg/L zeatin (PhytoTech, Cat No./ID: Z860-10ML), 3 mg/L $AgNO_3$ (Sinopharm Chemical Reagent, Cat No./ID: 81012365), and 7 g/L agar (Duchefa, Cat No./ID: P1001.0500), pH 5.8.

Shoot regeneration assays for *Solanum lycopersicum*

The shoot regeneration assays for *S. lycopersicum* were conducted as previously described, with some modifications[92]. First, seeds were washed in 75% ethanol for 1 min and then rinsed with sterile water five times. Next, seeds were treated with 50% bleach (2 drops of Tween-20 per 50 mL) for 10 min, followed by five more rinses in sterile water. The seeds were subsequently sown on the 1/2 MS agar plate and incubated in a RUIHUA incubator at 26 °C in the dark for 7–10 days. The hypocotyls of the seedlings were excised to a fixed length of approximately 1 cm and cultured on the CIM in the RUIHUA incubator at 26 °C in the dark for 14 days. If squeezing treatment is necessary, the excised hypocotyls were placed on a petri dish and gently squeezed with ophthalmic tweezers before being transferred to the CIM. To induce shoot regeneration, the resulting calli were transferred onto the SIM and cultured in the RUIHUA incubator at 26 °C under long-day conditions with a light intensity of 140 μmol m^{-2}·s^{-1}. The SIM was refreshed approximately every 17 days. U0126 was only applied during the CIM stage.

The formulation of the 1/2 MS agar medium is the same as that for *A. thaliana*. The formulation of CIM is as follows: 4.43 g MS basal medium w/vitamins powder (PhytoTech, Cat No./ID: M519-100L), 30 g/L sucrose (Abcone, Cat No./ID: S48029-1KG), 18 g/L mannitol (Sigma, Cat No./ID: M4125-500G), 2 mg/L 6-benzylaminopurine (PhytoTech, Cat No./ID: B130-100mL), 0.2 mg/L 1-naphthaleneacetic acid (PhytoTech, Cat No./ID: N605-100ML), 1:10000 ratio STS (0.1 M $Na_2S_2O_3$:0.1 M $AgNO_3$ = 4:1), and 7 g/L agar (Duchefa, Cat No./ID: P1001.0500), pH 5.8. The formulation of SIM is as follows: 4.43 g MS basal medium w/vitamins powder (PhytoTech, Cat No./ID: M519-100L), 30 g/L sucrose (Abcone, Cat No./ID: S48029-1KG), 1 mg/L zeatin (PhytoTech, Cat No./ID: Z860-10ML), and 2.5 g/L phytagel (Sigma, Cat No./ID: P8169-250G), pH 5.8.

Shoot regeneration assays for *Solanum pimpinellifolium*

The shoot regeneration assay for *S. pimpinellifolium* were conducted as described previously, with some modifications[92]. First, seeds were washed with 75% ethanol for 1 min and rinsed 5 times with sterile water. Next, seeds were treated with a 10% sodium hypochlorite solution (2 drops of Tween-20 per 50 mL) for 10 min, followed by five more rinses in sterile water. The seeds were subsequently sown on the 1/2 MS agar plate and cultured in an RUIHUA incubator at 26 °C in the dark for 5–7 days. The hypocotyls of seedlings were excised to a fixed length of approximately 1 cm and cultured on the CIM in a RUIHUA incubator at 26 °C in dark for 14 days. If squeezing treatment is required, the excised hypocotyls were placed on a petri dish and gently squeezed with ophthalmic tweezers, and then placed on the CIM. The calli were cultured on the SIM in a RUIHUA incubator at 26 °C under long-day conditions with a light intensity of 140 μmol m^{-2}·s^{-1}M stage.

The formulation of the 1/2 MS agar medium is the same as *A. thaliana*. The formulation of CIM is as follows: 4.43 g MS basal medium w/vitamins powder (PhytoTech, Cat No./ID: M519-100L), 30 g/L sucrose (Abcone, Cat No./ID: S48029-1KG), 18 g/L mannitol (Sigma, Cat No./ID: M4125-500G), 2 mg/L 6-benzylaminopurine (PhytoTech, Cat No./ID: B130-100mL), 0.2 mg/L 1-naphthaleneacetic acid (PhytoTech, Cat No./ID: N605-100ML), 1:10000 ratio STS (0.1 M $Na_2S_2O_3$:0.1 M $AgNO_3$ = 4:1), and 7 g/L agar (Duchefa, Cat No./ID: P1001.0500), pH 5.8. The formulation of SIM is as follows: 4.43 g MS basal medium w/vitamins powder (PhytoTech, Cat No./ID: M519-100L), 30 g/L sucrose (Abcone, Cat No./ID: S48029-1KG), 0.1 mg/L indole-3-acetic acid (PhytoTech, Cat No./ID: I364-100mL), 2 mg/L zeatin (PhytoTech, Cat No./ID: Z860-10ML), 2.5 g/L phytagel (Sigma, Cat No./ID: P8169-250G), pH 5.8. The formulation of the SIM for refreshment is as follows: 4.43 g MS basal medium w/vitamins powder (PhytoTech, Cat No./ID: M519-100L), 30 g/L sucrose (ABCONE, Cat No./ID: S48029-1KG), 1 mg/L zeatin (PhytoTech, Cat No./ID: Z860-10ML), and 2.5 g/L phytagel (Sigma, Cat No./ID: P8169-250G), pH 5.8.

Shoot regeneration assays for *Capsicum annuum*

The shoot regeneration assays for *C. annuum* CM334 were conducted as previously described, with some modifications[93,94]. Briefly, seeds were washed in 75% ethanol for 1 min, followed by five rinses with sterile water. The seeds were then treated with a solution of 50% bleach (containing 2 drops of Tween-20 per 50 mL) for 10 min, after which they were rinsed five more times in sterile water. The seeds were subsequently sown on the 1/2 MS agar plate and incubated in a RUIHUA incubator at 26 °C under long-day conditions with a light intensity of 140 μmol m^{-2}·s^{-1} for 14 days. After germination, the cotyledons were excised and cultured on CIM in the RUIHUA incubator at 26 °C under long-day conditions with a light intensity of 70 μmol m^{-2}·s^{-1} for 14 days. To induce shoot regeneration, the resulting calli were transferred onto SIM and cultured in the RUIHUA incubator at 26 °C under long-day conditions with a light intensity of 140 μmol m^{-2}·s^{-1}, with the SIM being refreshed approximately every 2 weeks. U0126 was only applied during the CIM stage.

The formulation of the 1/2 MS agar medium is the same as that for *A. thaliana*. The formulation of CIM is as follows: 4.43 g MS basal medium w/vitamins powder (PhytoTech, Cat No./ID: M519-100L), 30 g/L sucrose (Abcone, Cat No./ID:

S48029-1KG), 4 mg/L 6-benzylaminopurine (PhytoTech, Cat No./ID: B130-100mL), 3 mg/L indole-3-acetic acid (PhytoTech, Cat No./ID: I364-100mL), 7 g/L agar (Duchefa, Cat No./ID: P1001.0500), pH 5.8. The formulation of SIM is as follows: 4.43 g MS basal medium w/vitamins powder (PhytoTech, Cat No./ID: M519-100L), 30 g/L sucrose (Abcone, Cat No./ID: S48029-1KG), 4 mg/L 6-benzylaminopurine (PhytoTech, Cat No./ID: B130-100mL), 1 mg/L indole-3-acetic acid (PhytoTech, Cat No./ID: I364-100mL), 7 g/L agar (Duchefa, Cat No./ID: P1001.0500), pH 5.8.

Shoot regeneration assays for *Medicago sativa*

The shoot regeneration assays for *M. sativa* Zhongmu No.1 were conducted as previously described, with some modifications[95]. Briefly, seeds were washed in 75% ethanol for 1 min and then rinsed with sterile water five times. The seeds were then treated with 15% sodium hypochlorite solution (2 drops of Tween-20 per 50 mL) for 10 min, followed by five more rinses in sterile water. The seeds were subsequently sown on the 1/2 MS agar plate and incubated in a RUIHUA incubator at 26 °C in the dark for 5–7 days. After germination, the hypocotyls were excised to a fixed length of approximately 1 cm and cultured on CIM in a RUIHUA incubator at 26 °C in dark for 6 weeks, with the CIM being refreshed approximately every 3 weeks. To induce shoot regeneration, the resulting calli were transferred onto SIM and cultured in the RUIHUA incubator at 26 °C under long-day conditions with a light intensity of 140 μmol m^{-2}·s^{-1}. The SIM was refreshed approximately every 2 weeks until as many green proembryos as possible appeared. The calli were then transferred to hormone-free MS medium containing 20 g/L sucrose. U0126 was only applied during the CIM stage.

The formulation of the 1/2 MS agar medium is the same as *A. thaliana*. The formulation of CIM is as follows: 4.43 g MS basal medium w/vitamins powder (PhytoTech, Cat No./ID: M519-100L), 30 g/L sucrose (Abcone, Cat No./ID: S48029-1KG), 4 mg/L 2,4-dicholorophenoxyacetic acid (PhytoTech, Cat No./ID: D295-100mL), 0.5 mg/L kinetin (PhytoTech, Cat No./ID: K483-100mL), 7 g/L agar (Duchefa, Cat No./ID: P1001.0500), pH 5.8. The formulation of SIM is as follows: 4.43 g MS basal medium w/vitamins powder (PhytoTech, Cat No./ID: M519-100L), 30 g/L sucrose (Abcone, Cat No./ID: S48029-1KG), 1 mg/L kinetin (PhytoTech, Cat No./ID: K483-100mL), 0.5 mg/L 6-benzylaminopurine (PhytoTech, Cat No./ID: B130-100mL), 7 g/L agar (Duchefa, Cat No./ID: P1001.0500), pH 5.8.

Shoot regeneration assays for *Setaria viridis*

The shoot regeneration assays for *S. viridis* ME034V were conducted as previously described, with some modifications[96]. Briefly, the dehusked seeds were sterilized in a solution of 10% bleach plus 0.1% Tween-20 for 10 min on a rotating mixer, followed by five more rinses in sterile water. Excess water was then removed, and the sterilized seeds were dried on sterile filter paper. The seeds were subsequently cultured on CIM in a RUIHUA incubator at 26 °C with a photoperiod of 16 h for 1 week with a light intensity of 70 μmol m^{-2}·s^{-1} followed by 4–5 weeks in the dark, with the CIM being refreshed approximately every 2 weeks. To induce shoot regeneration, the resulting calli were transferred onto SIM and cultured in the RUIHUA incubator at 26 °C under long-day conditions with a light intensity of 140 μmol m^{-2}·s^{-1}, with the SIM being refreshed approximately every 2 weeks. U0126 was only applied during the dark treatment phase at the CIM stage.

The formulation of CIM is as follows: 4.43 g MS basal medium w/vitamins powder (PhytoTech, Cat No./ID: M519-100L), 40 g/L maltose (BBI, Cat No./ID: A604950-0500), 2 mg/L 2,4-dicholorophenoxyacetic acid (PhytoTech, Cat No./ID: D295-100mL), 0.5 mg/L kinetin (PhytoTech, Cat No./ID: K483-100mL), 0.6 mg/L copper sulfate pentahydrate (Sigma, Cat No./ID: C3036-250G), 4 g/L Gelzan (Sigma, Cat No./ID: G1910-250G), pH 5.8. The formulation of SIM is as follows: 4.43 g MS basal medium w/vitamins powder (PhytoTech, Cat No./ID: M519-100L), 20 g/L sucrose (Abcone, Cat No./ID: S48029-1KG), 1 mg/L 2,4-dicholorophenoxyacetic acid (PhytoTech, Cat No./ID: D295-100mL), 1 mg/L kinetin (PhytoTech, Cat No./ID: K483-100mL), 0.6 mg/L Copper sulfate pentahydrate (Sigma, Cat No./ID: C3036-250G), 7 g/L agar (Duchefa, Cat No./ID: P1001.0500), pH 5.8.

Shoot regeneration assays for *Oryza sativa*

The shoot regeneration assays for *O. sativa* ZH11 were conducted as previously described, with some modifications[97]. Briefly, the dehusked seeds were washed in 75% ethanol for 1 min and then rinsed with sterile water five times. The seeds were then treated with 20% sodium hypochlorite solution (2 drops of Tween-20 per 50 mL) for 15 min, followed by five more rinses in sterile water. Excess water was then removed, and the sterilized seeds were dried on sterile filter paper. The seeds were subsequently cultured on CIM in a RUIHUA incubator at 26 °C in dark for 6 weeks, with the CIM being refreshed approximately every 3 weeks. To induce shoot regeneration, the resulting calli were transferred onto SIM and cultured in the RUIHUA incubator at 26 °C under long-day conditions with a light intensity of 140 μmol m^{-2}·s^{-1}, with the SIM being refreshed approximately every 2 weeks. U0126 was only applied during the dark treatment phase at the CIM stage.

The formulation of CIM is as follows: 4.43 g NB basal medium w/vitamins powder (PhytoTech, Cat No./ID: N492-50L), 30 g/L sucrose (Abcone, Cat No./ID: S48029-1KG), 0.5 g/L L-Proline (Sigma, Cat No./ID: P5607-100G), 0.5g/L L-Glutamine (Sigma, Cat No./ID: G8540-100G), 0.3g/L Casamino acids (Caisson, Cat No./ID: C004-100GM), 2.5 mg/L 2,4-dicholorophenoxyacetic acid (PhytoTech, Cat No./ID: D295-100mL), 3.5 g/L phytagel (Sigma, Cat No./ID: P8169-250G), pH 5.8. The formulation of SIM is as follows: 4.43 g MS basal medium w/vitamins powder (PhytoTech, Cat No./ID: M519-100L), 30 g/L sucrose (Abcone, Cat No./ID: S48029-1KG), 30 g/L sorbitol (Abcone, cat No./ID: S18766-500G), 0.5 g/L L-Proline (Sigma, Cat No./ID: P5607-100G), 0.5g/L L-Glutamine (Sigma, Cat No./ID: G8540-100G), 0.3g/L Casamino acids (Caisson, Cat No./ID: C004-100GM), 0.1 g/L myo-inositol (BBI, Cat No./ID: A600536-0100), 2 mg/L kinetin (PhytoTech, Cat No./ID: K483-100mL), 2 mg/L 6-benzylaminopurine (PhytoTech, Cat No./ID: B130-100mL), 0.2 mg/L indole-3-acetic acid (PhytoTech, Cat No./ID: I364-100mL), 0.2 mg/L 1-naphthaleneacetic acid (PhytoTech, Cat No./ID: N605-100ML), 3.5 g/L phytagel (Sigma, Cat No./ID: P8169-250G), pH

5.8.

scRNA-seq library construction

The protoplasts of explants and calli were prepared as previously described with modifications[47]. Briefly, the hypocotyls (CIM0) and calli (CIM1–CIM7) were harvested and cut into small pieces using scissors. Each sample was then separately digested in an RNase-free enzyme solution consisting of 1.5% cellulase R10, 0.4% macerozyme R10, 0.5% snailase, 1% Driselase, 0.4 M mannitol, 0.1 M 4-morpholineethanesulfonic acid, 10 mM KCl, 10 mM $CaCl_2$, and 0.1% BSA, at room temperature for 2 h. During the enzymatic digestion, a syringe was used to mechanically disrupt the calli under a dissecting microscope to accelerate the digestion process. To completeness of digestion was confirmed under a stereomicroscope. The protoplasts were then filtered 3–4 times using cell strainers (40 μm in diameter, Falcon, Cat No./ID: 352340), concentrated, and washed 3–4 times with 8% mannitol at room temperature. Protoplast viability was assessed by trypan blue staining, with the ratio of viable cells to total cells in each sample exceeding 85%. The protoplast suspension was counted by a hemocytometer, and the final concentration of protoplasts was adjusted to 1,500–2,000 cells/μL.

scRNA-seq libraries were prepared as previously described[47]. Briefly, the cell suspensions were loaded onto a Chromium Single Cell Instrument (10× Genomics, USA) to generate single-cell GEMs. The scRNA-seq libraries were then constructed using the Chromium Single Cell 3′ Gel Bead and Library Kit v3 (10× Genomics, Cat No./ID: P/N 1000075 and 1000073). The detailed experimental procedure followed the user guide for the Chromium Single Cell 3′ Reagent Kits v3 (CG000183 Rev A). Qualitative analyses of DNA libraries were performed using an Agilent 2100 Bioanalyzer. The libraries were sequenced on an Illumina NovaSeq X Plus (Shanghai Genomics Technology, China) using two 150 bp paired-end kits. The resulting raw scRNA-seq data comprised 28 bp Read1, 150 bp Read2, and 8 bp i7 index reads.

Identification of protoplasting-responsive genes

To minimize the impact of protoplasting on scRNA-seq, we performed RNA-seq on calli at four time points. The bulk RNA-seq data on the samples at CIM0, 3, and 7 without protoplasting were described[38]. By comparing differentially expressed genes between normal condition and protoplast, we identified protoplasting-responsive genes at each time point (log_2FoldChange > 2 and *padj* < 0.05) (Supplementary Fig. S1b). The resulting shared set of 284 genes was used as the final gene list (Supplementary Table S1). We then mitigated the effect of protoplasting on scRNA-seq by filtering these genes (see below).

Pre-processing of raw scRNA-seq data

The raw scRNA-seq data were initially processed using Cell Ranger (v7.0.0, 10× Genomics, USA). This software pipeline includes aligning reads and generating gene-cell matrices from the raw scRNA-seq data. The genome and GTF annotation files of *A. thaliana* were obtained from TAIR (arabidopsis.org/), specifically using the TAIR10 version of the genome and the Araport11 version of the annotation files. To build the reference, we executed the "cellranger mkref" command with the "--genome, --fasta and –genes" arguments. Subsequently, we ran the "cellranger count" command with the "--id, --transcriptome, --fastqs, --sample" arguments to generate single-cell gene counts. The gene-cell matrices directory generated by Cell Ranger (v7.0.0), named "filtered_feature_bc_matrix" by 10× Genomics, served as the raw data for further analysis.

scRNA-seq data analysis for a single sample

Single-cell data analyses were conducted following the guidelines outlined in the Bioconductor community's manual, "Orchestrating Single-Cell Analysis with Bioconductor (OSCA)"[98]. First, we used the "read10xCounts" function from the DropletUtils package (v1.16.0) to import the single-cell expression matrix obtained from Cell Ranger, converting it into a SingleCellExperiment object. Next, we applied the "scDblFinder" function from the scDblFinder package (v1.10.0) to identify doublets within the dataset[99]. Following this, we conducted a data quality assessment using the "perCellQCMetrics" and "addPerCellQCMetrics" functions from the scuttle package (v1.6.2). Subsequently, we performed cell outlier detection based on the quality metrics obtained in the previous step using the "isOutlier" function from the robustbase package (v0.95). We filtered cells based on their classification as outliers, the proportion of chloroplast and mitochondrial content (with a threshold set at 5%), and the presence of doublets.

We used the "quickCluster" function from the scran package (v1.24.0) for rapid cell clustering. Following the clustering, we applied the "computeSumFactors" function to adjust for sequencing depth in each cell, resulting in a factor-scaled and log-transformed single-cell expression matrix. Finally, we utilized the "modelGeneVar" function from the scran package (v1.24.0) to model the variation of each gene across different cells, identifying the top 1,000 highly variable genes for subsequent analysis. Among these highly variable genes, we removed protoplast-responsive genes to mitigate the effects of protoplasting on our data.

We employed the "runPCA" function from the scater package (v1.27.9) to perform dimensionality reduction on the single-cell data. Following this, we used the "runTSNE" and "runUMAP" functions, also from the scater package (v1.27.9), to create *t*-SNE and UMAP plots for visualization. Subsequently, we applied the "clusterCells" function from the scran package (v1.24.0) to cluster all cells in the atlas according to the PCA results. We selected the "Louvain" method for clustering and used the "jaccard" method for boundary weight calculations. We experimented with different numbers of neighboring cells — specifically 5, 10, 20, and 50 — to obtain varying cluster counts, selecting specific cluster numbers based on our annotation requirements. Finally, we utilized the "scoreMarkers" function from the scran package (v1.24.0) to calculate marker genes for each cell cluster. To assist in identifying marker genes, we also calculated a score using the results generated by the "scoreMarkers" function. The scoring formula is as follows: "score = (self.average – other.average) / (other.average + 1e-5) * median.logFC.detected". We defined candidate marker genes as those with self.detected > 0.05 and self.average – other.average > 0, along with the highest scores.

Two biological replicates were performed for each time point except CIM7 (Supplementary Table S1). The integration of the callus atlas at CIM7 (from this study) with the published atlas at CIM6 revealed a high degree of similarity (Supplementary Fig. S3j)[32].

Integrated analysis of scRNA-seq data for multi-samples

We utilized the "multiBatchNorm" function from the batchelor package (v1.12.3) to correct for sequencing depth across the single-cell data as mentioned above, allowing for integration across multiple samples. Following this, we employed the "combineVar" function from the same batchelor package to integrate the highly variable genes identified in the above single simple analysis, resulting in a consolidated set of highly variable genes. From this set, we selected the top 6,000 genes for subsequent data analysis. The protoplast-responsive genes were removed during this process.

Next, we performed dimensionality reduction on the corrected single-cell data using the "runPCA" function, followed by visualization with "runTSNE" and "runUMAP". We assessed the results from *t*-SNE and UMAP to determine if further integration was necessary, avoiding the risk of over-integration. In case where multiple samples could not be effectively integrated in the *t*-SNE or UMAP plots, we applied the "fastMNN" function from the batchelor package (v1.12.3) for integration. The order of merging was based on our sample choice: for samples derived from calli at multiple time points, we merged them in the order of CIM 0, 1, 3, and 7; for a comparison of a control group with a treatment group, the merging occurred in the order of control followed by treatment.

For further data visualization, we selected the "corrected "dimensions in the "dimred" option of the "runTSNE" and "runUMAP" functions. We subsequently employed the "clusterCells" function to conduct clustering on the integrated single-cell data. If the integration was achieved using fastMNN, we specified the "corrected" dimensions in the "use.dimred" option; otherwise, we used the "PCA" dimensions. The remaining clustering parameters remained consistent with those used in the above "scRNA-seq data analysis for a single sample" section.

Finally, if multiple samples represented multiple biological replicates, we activated the "block" option in the "scoreMarkers" function when calculating marker genes. This enabled us to fully leverage the replicate information, thereby enhancing the identification of robust marker genes across biological replicates.

Chemical screening

We used liquid CIM media for chemical screening in 24-well plates based on three main reasons: 1) Using normal Petri dishes (9 cm × 9 cm) would require large quantities of each compound, increasing costs and making large-scale screening impractical; 2) It is difficult to evenly distribute compounds in solid CIM medium in 24-well plates; 3) Using solid media in a 24-well plate risks cross-contamination from tweezers when placing explants in different compounds, affecting results. In contrast, using liquid media allows us to add compounds after placing the explants, avoiding cross-contamination.

The chemical compound library (Selleck New Compound Library) was obtained from Core Technology Facility of Center (CAS Center for Excellence in Molecular Cell Science, sjzx.sibcb.ac.cn/Cn/Index/listView/catid/58.html) (Supplementary Table S1). The steps for compound screening are as follows (Supplementary Fig. S12f): 1) Preparation of Culture Plates: add 1.8 mL of liquid CIM to each well of a 24-well cell culture plate, and then place eight hypocotyl explants into each well; introduce 0.9 μL of a 10 mM stock solution of the compound to each well, while designating one well on each plate as a control by adding 0.9 μL of DMSO. 2) Incubation: seal the cell culture plates with Parafilm to prevent contamination and incubate them in a Percival incubator at 22 °C under long-day conditions, with a light intensity of 45 μmol $m^{-2}{\cdot}s^{-1}$ for 7 days. 3) Fluorescence Observation: use a confocal microscope to examine the number of *pACL5::sGFP-N7* fluorescence foci in the calli treated with DMSO; establish the threshold by identifying the lowest number of fluorescent foci observed in 8 calli; subsequently, evaluate the fluorescence in the callus treated with each compound. If the count of fluorescent foci exceeds the threshold, record it as 1; if it falls below the threshold, record it as 0. 4) Selection of Promising Compounds: choose the compounds with the highest number of 0s for a second round of screening. The protocol for the second round follows the same method as the first round. 5) Selection of Candidate Compounds: after completing both rounds of screening, select candidate compounds for statistical analysis of fluorescence foci on the CIM and assess their shoot regeneration efficiency on the SIM. 6) Validation of Candidate Compounds I: add 5 μM of the candidate compound to the CIM and place 24 explants. After 7 days of culture, count the number of fluorescent foci in each callus and capture representative images. 7) Validation of Candidate Compounds II: add 5 μM of the candidate compound to the CIM. After 7 days of culture, transfer the explants to the SIM. After 16 days of culture, count the number of roots and shoots produced.

The chemical compound library of MEK inhibitors was obtained from TargetMol (Supplementary Table S1). The steps for compound screening followed the previously described protocol, with one exception: during the fluorescent observation step, we utilized a larger quantity of calli (n = 15 instead of 8) for each MEK compound. This adjustment allowed us to more effectively identify MEK inhibitors with stronger effects.

Frozen sectioning

To prepare frozen sections of fresh callus tissues for *in situ* RNA sequencing (IISS), follow these steps: 1) Immerse fresh callus tissues in Optimal cutting temperature compound (OCT) (Skura, Cat No./ID:4583) and apply a vacuum for 1–2 minutes while on ice, ensuring that no bubbles form. 2) Add an appropriate amount of OCT into an embedding mold (Citotest, Cat No./ID: 80203-0007). Then, transfer the tissue onto the surface of the OCT. 3) Quickly place the mold containing the tissue onto dry ice until the material solidifies. 4) Use a cryostat (Leica CM3050S) for sectioning, setting the blade temperature to −15 °C and the chamber temperature to −20 °C. Slice the tissue into sections with a thickness of 10 μm. 5) Lay the tissue slices flat on low-adhesion glass slides (Citotest, Cat No./ID: 188105) for further analysis.

In situ RNA sequencing

The IISS was performed as previously described[51]. In brief, fresh frozen sections underwent an initial treatment at 37 °C for 5 min, followed by fixation in 4% (w/v) paraformaldehyde for 5 min. The sections were then washed twice with diethyl pyrocarbonate (DEPC)-treated 1× phosphate buffered saline (PBS). Subsequently, the sections were dehydrated through a series of ethanol concentrations, followed by three washes with Wash Buffer (Dynamic Biosystems, Suzhou, China), and then treated with 0.1 M HCl at 37 °C for 5 min.

The sections were incubated sequentially with the following solutions: custom target gene probes (Dynamic Biosystems, Suzhou, China) labeled with a specific barcode for each RNA molecule in hybridization mix at 37 °C for 4 h, a ligation mix at 37 °C for 30 min, splint primers in a circularization mix at 37 °C for 30 min, and an amplification mix for rolling circle amplification at 30 °C overnight. After each incubation step, the slides were washed three times with Wash Buffer at room temperature.

For sequencing, the sections were incubated in ligation buffer containing anchor primers, labeled sequencing interrogation probes, and ligase at 30 °C for 45 min. They were then mounted with SlowFade Gold Antifade Mountant (ThermoFisher, Cat No./ID: S36938) mixed with 0.5 μg/mL 4',6-diamidino-2-phenylindole (DAPI). Imaging was conducted using a 3D-Hitech Pannoramic® MIDI II equipped with a pco.edge 4.2 bi-camera, utilizing a 20× objective lens. A reference image was established through a round of DAPI imaging, and the SIFI algorithm was employed to extract features from different rounds of DAPI images. Corresponding feature points across rounds were matched, and these matched points were used for affine transformation to register images from various rounds. Background filtering was performed using the "tophat" function from OpenCV. By distinguishing genuine signals and decoding them, the spatial localization and quantification of RNAs were ultimately attained. The analytical pipeline utilized in this study can be accessed at github.com/DynamicBiosystems/DynamicISS.

Tissue embedding and sectioning

Samples were collected and immediately placed in the vials with ice-cold PBS containing 2.5% paraformaldehyde (PFA, pH 7.0). The samples were infiltrated for 30 min by vacuum at ice. Tissues were then washed with PBS solution for three times, embedded with 6% low melting agarose, and sliced with a Lecia Sliding Microtome 1200S at the thickness of 70 to 130 μm.

Cell outline staining

For the hypocotyl (CIM0) and calli at different stages (CIM1 to CIM5), transfer the samples into water containing propidium iodide (PI, Meilunbio, Cat No./ID: MA0137_1ML) at a concentration of 5–10 μg/mL. Incubate at room temperature for 5–10 minutes, then rinse three times with water. For the calli at CIM7, first fix the samples using 2.5% PFA as described above. Then transfer the samples to ClearSee solution[100], and incubate overnight at room temperature. Add SCRI Renaissance 2200 (SR2200, Renaissance Chemicals, Cat No./ID: SR2200) reagent to the ClearSee solution to a final concentration of 0.1%, and incubate for 1 h at room temperature. Afterwards, wash the samples once with ClearSee solution.

Microscopy

For confocal imaging, we used FV3000 confocal microscopic system (Olympus, Japan). Proper filter sets and lasers were selected for fluorescence signal scanning. Specifically, sGFP and VENUS were stimulated with an argon laser at 488 nm, with emission filtered at 500 to 540 nm; DsRed was excited at 561 nm and detected at a wavelength between 570 to 620 nm; PI was excited at 561 nm and detected at a wavelength between 590 to 680 nm; SR2200 was excited at 405 nm and detected at a wavelength between 430 to 470 nm. The images were processed with ImageJ.

Time-lapse recording of callus development under white light conditions

We used FV3000 confocal microscopic system (Olympus, Japan) to conduct time-lapsed tracking of specific callus region of the fluorescence reporter lines. For each experiment, the callus was placed in a glass-bottom cell culture dish containing 300 μL of the SIM phytagel medium (Biosharp, Cat No./ID: BS-20-GJM). We labeled specific callus regions by marking the bottom of the dish. Once the tracking at each time point was complete, the callus was returned to the normal culture conditions.

We used BX63 microscope (Olympus, Japan) equipped with a DP74 digital camera for time-lapsed tracking of the entire callus. For each experiment, the callus was placed in a glass-bottom culture dish containing 300 μL of SIM phytagel medium. We used the "automatic XY-Positions/MIA acquisition process" function in OLYMPUS CellSens Dimension software (v4.1.1) to scan the entire callus and merged all the images into one stitched image. Once the tracking at each time point is complete, the callus is returned to the normal culture condition.

Time-lapse recording of ACL5$^+$ callus regions

We combined SpinSR spinning-disk microscope (Olympus, Japan) and BX63 microscope (Olympus, Japan) for time-lapse tracking of ACL5$^+$ callus regions. The ACL5$^+$ callus regions were defined as those exhibiting a striped expression pattern of *ACL5* (Supplementary Fig. S7b). Specifically, we used SpinSR spinning-disk microscope, which shortens imaging time and minimizes phototoxicity, to define the ACL5$^+$ and ACL5$^-$ callus regions at CIM7 and employed the "automatic XY-Positions/MIA acquisition process" function in OLYMPUS CellSens Dimension software (v4.3) of SpinSR to scan the entire callus and merged all the images into one stitched image. During the SIM stages, we used BX63 microscope for time-lapsed tracking of the corresponding callus regions and used the "automatic XY-Positions/MIA acquisition process" function in OLYMPUS CellSens Dimension software (v4.1.1) of BX63 to scan the entire callus and merged all the images into one stitched image. By comparing the ACL5$^+$ and ACL5$^-$ callus regions at CIM7 with the corresponding callus regions at the SIM stages, we determined their cell fates. For each experiment, the callus was placed in a glass-bottom cell culture dish containing 300 μL of the SIM phytagel medium (Biosharp, Cat No./ID: BS-20-GJM). Once the tracking at each time point was complete, the callus was returned to the normal culture

conditions. Fluorescence acquisition settings for *pACL5::sGFP-N7* reporter: 488-nm excitation; emission collected at 500–550 nm.

Live and time-lapse imaging using fluorescent reporters

A 35-mm glass-bottom dish was pre-rinsed with 200 µL of 0.1% BSA to reduce surface tension. To minimize any impact of medium on fluorescence imaging, 50 µL of solid CIM medium was used. After the medium solidified, callus tissue was placed on the surface. The tissue was overlaid with a thin layer of 1% agar, followed by 200 µL of liquid CIM medium.

Live imaging with PlaCCI was performed at room temperature on SpinSR spinning-disk confocal microscope (Olympus, Japan) at 40-minute intervals for a total of 66 cycles. Z-stacks were acquired with a step size of 3 µm. Fluorescence acquisition settings: *pCDT1a::CDT1a-eCFP*: 445-nm excitation; emission 465–495 nm. *pHTR13::HTR13-mCherry*: 561-nm excitation; emission 565–595 nm. *pCYCB1;1::NCYCB1;1-YFP*: 488-nm excitation; emission 500–550 nm.

Time-lapse imaging with *pAT2G18020:H2B-mCherry* and Cytrap was performed at room temperature on FV3000 microscope (Olympus, Japan), with Z-stacks acquired eight times daily. After tracking at each time point was completed, the callus was returned to normal culture conditions. The fluorescence acquisition settings for *pAT2G18020:H2B-mCherry* and *pCYCB1::CYCB1-GFP* were the same as those described above.

EdU labeling experiment

For the 5-ethynyl-2'-deoxyuridine (EdU) labeling experiments, calli at different growth stages were transferred to a small dish containing liquid CIM, 10 µM of EdU, and 5 µM of U0126 (with DMSO as a control). After incubating for 4 h at 22 °C (or 8 h for the explants at CIM0), the culture media were replaced with 1 mL of fix solution (4% PFA). The samples were then subjected to vacuum infiltration for 15 min and washed twice with 1 mL of wash buffer (PBS containing 3% BSA) for 3–5 min each. Subsequently, 1 mL of permeabilization buffer (PBS containing 0.3% Triton X-100) was added into each well, and the samples were incubated at room temperature for 10–15 min. The calli were washed 1–2 times with 1 mL of wash solution for 3–5 min each. The remaining procedures were performed using EdU Cell Proliferation Kit (Beyotime, Cat No./ID: C0071S) according to the manufacturer's instructions.

RNA-seq experiments

Total RNAs were extracted from calli using RNeasy Plant Mini Kit (Qiagen, Cat No./ID: 74904). Library construction and 150-bp paired-end sequencing were performed using the Illumina NovaSeq X plus Platform according to manufacturer's protocols (Personal Biotechnology, Shanghai, China). Two or three biological replicates were performed.

Data preprocessing and reads alignment for RNA-seq

For each library, raw.fastq was first trimmed by fastp (v0.20.0)[101] with default parameters. FastQC (v0.11.7) and MulitQC (v1.6) were then performed to obtain clean fq files[102]. Reads were finally aligned to the *A. thaliana* (TAIR10), *B. napus* (ZS11), and *S. pimpinellifolium* (LA1589) genomes using hisat2 (v2.1.0)[103]. The TAIR10 genome sequence was downloaded from TAIR. The ZS11 and LA1589 genome sequences were downloaded from BnPIR[104] and Figshare[105], respectively. The resulting SAM files were converted into the BAM format, sorted, and indexed by Samtools (v1.9)[106].

RNA-seq data analyses

The number of paired mapping reads overlapping each annotated gene (*A. thaliana*: *Araport11*; *B. napus*: *ZS11*; *S. pimpinellifolium*: *LA1589*) was quantified using featureCounts (v1.6.2) with the parameter "-p"[107,108]. The resulting counts files served as inputs for differential gene expression analysis performed with DESeq2 (v1.36.0)[109]. Log fold change shrinkage was estimated using the ashr package[110].

For data visualization, we extracted the normalized count values generated by DESeq2 and applied max-min scaling. Gene Ontology (GO) and Gene Set Enrichment Analysis of differentially expressed genes were conducted using clusterProfiler (v4.4.1)[111] and org.At.tair.db (v3.15.1). The Plant Ontology (PO) set was downloaded from the Planteome github repository[112], and the gene-PO annotations were sourced from TAIR. We used ontologyIndex (v2.12)[113] to select sets of ontological terms, and the "enricher" function provided by ClusterProfiler (v4.4.1) to conduct PO enrichment analysis.

Mass-spectrometry-based phosphoproteomic analysis

Callus tissues were treated with either DMSO (mock) or U0126 for 7 days on CIM, with each biological replicate weighing between 0.1 and 0.2 grams. Total protein was extracted with 6 M guanidine hydrochloride buffer (100 mM Tris-HCl, 10 mM EDTA, 10 mM TCEP, 1 mM PMSF, pH 8.0) and quantified by bicinchoninic acid (BCA) assay. Two milligrams of protein were digested overnight at 37 °C with trypsin (Promega, Cat. No./ID: V5280). Peptides were quantified, allocating 10 µg for global proteomics and 1.5 mg for phosphoproteomics. Phosphopeptides were enriched using the High-Select TiO2 Phosphopeptide Enrichment Kit (Thermo Fisher Scientific, Cat No./ID: A32993) according to the manufacturer's instructions. LC-MS/MS was performed on a timsTOF Pro 2 mass spectrometer (Bruker Daltonics) in data-independent acquisition (DIA) mode with parallel accumulation–serial fragmentation (PASEF). Raw data were processed in Spectronaut 19 (Biognosys) with default settings for label-free quantification against the *A. thaliana* reference proteome (UniProt UP000006548). Five biological replicates were performed.

Phosphoproteomics mass spectrometry data analysis

We used the NAguideR package (v0.2.1) to perform missing value imputations and ensure data quality for both proteomics and phosphoproteomics datasets. The data were then transformed to log2 scale for subsequent analysis and statistical evaluation[114]. To correct for variations, we adjusted the phosphopeptide data by dividing the abundance of phosphopeptides by the corresponding abundance of their respective proteins. Differential analysis of the corrected phosphopeptides was carried out using the limma package (v3.58.1)[115]. For GO term analysis of the differentially expressed phosphopeptides, we employed clusterProfiler (v4.4.1)[111] and org.At.tair.db (v3.15.1). Additionally, we conducted motif enrichment analysis of the differential phos-

phopeptides using pLogo[116] and motif-x 2.0[117].

Quantification and statistical analysis

For Fig. 2d, a generalized linear mixed model (GLMM) with a generalized Poisson distribution was fitted using the glmmTMB package to account for underdispersion and repeated measurements, with material type, time point, and their interaction treated as fixed effects, and explant (Callus) and individual tracking ID (Location) treated as random effects. Model residuals were validated using the DHARMa package, showing acceptable dispersion and overall distribution fit. Post-hoc pairwise comparisons between ACR and FCR at each specific day were subsequently conducted based on estimated marginal means using the emmeans package, with *P* values adjusted for multiple testing using the False Discovery Rate (FDR) method.

For Fig. 2e, to evaluate the initiation timing of cell division, a mixed-effects Cox proportional hazards model was applied with the explant batch (Callus) included as a random effect. The results revealed that ACR initiated division (reaching ≥ 2 cell layers) significantly earlier than FCR ($P < 0.001$, $z = 11.84$). The hazard ratio (HR) for ACR relative to FCR was 11.98 (95% CI: 7.94–18.07), indicating that ACR cells progressed to two or more layers at an approximately 12-fold higher rate compared to FCR.

For Fig. 2f, to compare the proportion of cells undergoing the first division between ACR and FCR across time points (CIM1, CIM2, and CIM3), a linear mixed-effects model (LMM) was fitted using the lme4 and lmerTest packages in R. The model included material type (ACR vs FCR), time point (Day), and their interaction (type × Day) as fixed effects, while individual explant batches (CallusID) were treated as a random intercept to account for the paired experimental structure. Pairwise comparisons between ACR and FCR at each specific day were performed using estimated marginal means via the emmeans package, with *P* values adjusted for multiple testing using the False Discovery Rate (FDR / Benjamini-Hochberg) method.

We used Student's *t*-test or one-way ANOVA and Tukey's multiple comparisons to determine the statistical significance between different samples in quantification and phenotypes. All statistical results and graphs were generated by R. The numbers of samples and types of statistical analyses are given in figure legends. The normality of the data distribution and the homogeneity of variances (homoscedasticity) were evaluated using the Shapiro–Wilk test or Levene's test, respectively. Based on the evaluation results, appropriate parametric tests (e.g., Student's *t*-test and ANOVA) or non-parametric tests (e.g., Mann–Whitney U test and Kruskal–Wallis test) were applied for subsequent comparisons.

DATA AVAILABILITY

The scRNA-seq and RNA-seq data (BioProject PRJCA034290) were deposited in Beijing Institute of Genomics Data Center (bigd.big.ac.cn). The raw data related to phosphoproteomics and spatial transcriptomics were deposited on Figshare through doi.org/10.6084/m9.figshare.33159995.

ACKNOWLEDGEMENTS

We thank Prof. Zhi-Hong Xu (CEMPS, CAS, China) for valuable comments, Dr. Eekhout Thomas and Dr. Bert De Rybel (VIB Center for Plant Systems Biology, Belgium) for providing root cell atlas data, Dr. Crisanto Gutierrez (Centro de Biologia Molecular Severo Ochoa, Spain) for PlaCCI seeds, Dr. Masaaki Umeda (Nara Institute of Science and Technology, Japan) for Cytrap seeds, Dr. Juan Xu (Zhejiang University, China) for the conditional *mpk3/6* mutants, Dr. Chao-Feng Huang (CEMPS, CAS, China) for the *mkk1/2* mutant, Dr. Tongda Xu (Fujian Agriculture and Forestry University, China) for *mkk4,5RNAi*-est line, Dr. Jianghua Chen (Xishuangbanna Tropical Botanical Garden, CAS, China) for *M. sativa* seeds, Dr. Ying-Juan Cheng and Dr. Tian-Qi Zhang (Nanjing Agriculture University, China) for tomato seeds, Dr. Yan-Xia Mai, Dr. Wen-Juan Cai, Shan-Shan Wang, and Jin-Juan Bai (Core Facility of CEMPS, CAS) for technical support in flow cytometry analysis, imaging, phosphoproteomic analysis, and regeneration assays, Core Technology Facility of Center from CAS Center for Excellence in Molecular Cell Sciences for Selleck New Compound Library, Mrs. Yu Chen for proposing n-hexane treatment, Mrs. Ren-Yu Liao for her advice on long-term live imaging, Dr. Caixia Gao (Institute for Genetics and Developmental Biology, CAS, China) for sharing unpublished data, and Dr. Lu Yuan (Xianghu Laboratory, China) for assistance in crop regeneration experiments. This work was supported by the grants from Biological Breeding-National Science and Technology Major Project (2024YFF1000703) to H.L., the National Natural Science Foundation of China (32388201; 32400292) to J.-W.W. and F.-X.W., Strategic Priority Research Program of the Chinese Academy of Sciences (XDB0630201; XDB0630301) to J.-W.W. and B.L., CAS-ANSO Co-funding Research Project (CAS-ANSO-CFRP-2024-07) to J.-W.W., Key Research and Development Program of Zhejiang Province to G.-D.S., and the New Cornerstone Science Foundation through the XPLORER PRIZE to J.-W.W., and Shanghai Postdoctoral Excellence Program (2021391) to F.-X.W.

AUTHOR CONTRIBUTIONS

G.-D.S., F.-X.W., and J.-W.W. designed the research. F.-X.W., G.-D.S., L.-Y.W., and S.-Y.W. performed scRNA-seq experiments and analyzed promoter reporter lines. G.-D.S., F.-X.W., and S.-Q.L. performed shoot regeneration assays and chemical screen. F.-X.W. and H.L. performed spatial transcriptomics. G.-D.S., F.-X.W., and Z.-G.X. analyzed scRNA-seq data. B.L. provided advice on regeneration assays. J.-W.W. wrote the article.

COMPETING INTERESTS

The authors declare no competing interests.

REFERENCES

1. Birnbaum, K.D. & Sánchez Alvarado, A. Slicing across kingdoms: regeneration in plants and animals. *Cell* **132**, 697–710 (2008).
2. Sugimoto, K., Gordon, S.P. & Meyerowitz, E.M. Regeneration in plants and animals: dedifferentiation, transdifferentiation, or just differentiation? *Trends Cell Biol.* **21**, 212–218 (2011).
3. Eshed Williams, L. Genetics of shoot meristem and shoot regeneration. *Annu. Rev. Genet.* **55**, 661–681 (2021).
4. Shin, J., Bae, S. & Seo, P.J. *De novo* shoot organogenesis during plant regeneration. *J. Exp. Bot.* **71**, 63–72 (2020).

5. Duclercq, J., Sangwan-Norreel, B., Catterou, M. & Sangwan, R.S. *De novo* shoot organogenesis: from art to science. *Trends Plant Sci.* **16**, 597–606 (2011).
6. Ikeuchi, M. et al. Molecular mechanisms of plant regeneration. *Annu. Rev. Plant Biol.* **70**, 377–406 (2019).
7. Ibáñez, S., Carneros, E., Testillano, P.S. & Pérez-Pérez, J.M. Advances in plant regeneration: shake, rattle and roll. *Plants* **9**, 897 (2020).
8. Sang, Y.L., Cheng, Z.J. & Zhang, X.S. iPSCs: a comparison between animals and plants. *Trends Plant Sci.* **23**, 660–666 (2018).
9. Ikeuchi, M., Ogawa, Y., Iwase, A. & Sugimoto, K. Plant regeneration: cellular origins and molecular mechanisms. *Development* **143**, 1442–1451 (2016).
10. Liao, R.Y. & Wang, J.W. Analysis of meristems and plant regeneration at single-cell resolution. *Curr. Opin. Plant Biol.* **74**, 102378 (2023).
11. Chen, C.L. et al. Plant regeneration in the new era: from molecular mechanisms to biotechnology applications. *Sci. China Life Sci.* **67**, 1338–1367 (2024).
12. Yu, H. et al. A route to *de novo* domestication of wild allotetraploid rice. *Cell* **184**, 1156–1170.e14 (2021).
13. Altpeter, F. et al. Advancing crop transformation in the era of genome editing. *Plant Cell* **28**, 1510–1520 (2016).
14. Ikeuchi, M., Sugimoto, K. & Iwase, A. Plant callus: mechanisms of induction and repression. *Plant Cell* **25**, 3159–3173 (2013).
15. Doll, Y. & Ikeuchi, M. All roads lead to dome: multicellular dynamics during *de novo* meristem establishment in shoot regeneration. *Curr. Opin. Plant Biol.* **85**, 102733 (2025).
16. Mathew, M.M. & Prasad, K. Model systems for regeneration: *Arabidopsis*. *Development* **148**, dev195347 (2021).
17. Atta, R. et al. Pluripotency of Arabidopsis xylem pericycle underlies shoot regeneration from root and hypocotyl explants grown *in vitro*. *Plant J.* **57**, 626–644 (2009).
18. Che, P., Lall, S. & Howell, S.H. Developmental steps in acquiring competence for shoot development in *Arabidopsis* tissue culture. *Planta* **226**, 1183–1194 (2007).
19. Lu, X.Y. et al. Development of an inducible DNA barcoding system to understand lineage changes in *Arabidopsis* regeneration. *Dev. Cell* **60**, 305–319.e5 (2025).
20. Bagchi, R. et al. The *Arabidopsis* ALF4 protein is a regulator of SCF E3 ligases. *EMBO J.* **37**, 8 (2018).
21. DiDonato, R.J. et al. *Arabidopsis ALF4* encodes a nuclear-localized protein required for lateral root formation. *Plant J.* **37**, 340–353 (2004).
22. Sugimoto, K., Jiao, Y.L. & Meyerowitz, E.M. *Arabidopsis* regeneration from multiple tissues occurs via a root development pathway. *Dev. Cell* **18**, 463–471 (2010).
23. Ramirez-Parra, E. et al. The transcription factor *OBP4* controls root growth and promotes callus formation. *New Phytol.* **213**, 1787–1801 (2017).
24. Shang, B.S. et al. Very-long-chain fatty acids restrict regeneration capacity by confining pericycle competence for callus formation in *Arabidopsis*. *Proc. Natl. Acad. Sci. USA* **113**, 5101–5106 (2016).
25. Zhang, S.Q. et al. The calcium signaling module CaM-IQM destabilizes IAA-ARF interaction to regulate callus and lateral root formation. *Proc. Natl. Acad. Sci. USA* **119**, e2202669119 (2022).
26. Xu, C.Y. et al. Control of auxin-induced callus formation by bZIP59-LBD complex in *Arabidopsis* regeneration. *Nat. Plants* **4**, 108–115 (2018).
27. Fan, M.Z., Xu, C.Y., Xu, K. & Hu, Y.X. LATERAL ORGAN BOUNDARIES DOMAIN transcription factors direct callus formation in *Arabidopsis* regeneration. *Cell Res.* **22**, 1169–1180 (2012).
28. Xu, C.Y. et al. Transcriptional activation by WRKY23 and derepression by removal of bHLH041 coordinately establish callus pluripotency in *Arabidopsis* regeneration. *Plant Cell* **36**, 158–173 (2024).
29. Kareem, A. et al. *PLETHORA* genes control regeneration by a two-step mechanism. *Curr. Biol.* **25**, 1017–1030 (2015).
30. Bae, S.H., Noh, Y.S. & Seo, P.J. REGENOMICS: a web-based application for plant REGENeration-associated transcriptOMICS analyses. *Comput. Struct. Biotechnol. J.* **20**, 3234–3247 (2022).
31. Liu, J. et al. The *WOX11-LBD16* pathway promotes pluripotency acquisition in callus cells during de novo shoot regeneration in tissue culture. *Plant Cell Physiol.* **59**, 739–748 (2018).
32. Zhai, N. & Xu, L. Pluripotency acquisition in the middle cell layer of callus is required for organ regeneration. *Nat. Plants* **7**, 1453–1460 (2021).
33. Ogura, N. et al. WUSCHEL-RELATED HOMEOBOX 13 suppresses de novo shoot regeneration via cell fate control of pluripotent callus. *Sci. Adv.* **9**, eadg6983 (2023).
34. Lee, K. & Seo, P.J. Dynamic epigenetic changes during plant regeneration. *Trends Plant Sci.* **23**, 235–247 (2018).
35. Aflaki, F., Gutzat, R. & Mozgová, I. Chromatin during plant regeneration: opening towards root identity? *Curr. Opin. Plant Biol.* **69**, 102265 (2022).
36. He, C.S., Chen, X.F., Huang, H. & Xu, L. Reprogramming of H3K27me3 is critical for acquisition of pluripotency from cultured *Arabidopsis* tissues. *PLoS Genet.* **8**, e1002911 (2012).
37. Lee, S., Bae, S.H., Jeon, Y., Seo, P.J. & Choi, Y. DEMETER DNA demethylase reshapes the global DNA methylation landscape and controls cell identity transition during plant regeneration. *BMC Genomics* **25**, 1234 (2024).
38. Wu, L.Y. et al. Dynamic chromatin state profiling reveals regulatory roles of auxin and cytokinin in shoot regeneration. *Dev. Cell* **57**, 526–542.e7 (2022).
39. Hong, C. et al. Histone modification-dependent production of peptide hormones facilitates acquisition of pluripotency during leaf-to-callus transition in Arabidopsis. *New Phytol.* **242**, 1068–1083 (2024).
40. Shim, S. et al. Dynamic changes in DNA methylation occur in TE regions and affect cell proliferation during leaf-to-callus transition in Arabidopsis. *Epigenetics* **17**, 41–58 (2022).
41. Shim, S., Lee, H.G. & Seo, P.J. MET1-dependent DNA methylation represses light signaling and influences plant regeneration in *Arabidopsis*. *Mol. Cells* **44**, 746–757 (2021).
42. Yan, A., Borg, M., Berger, F. & Chen, Z. The atypical histone variant H3.15 promotes callus formation in *Arabidopsis thaliana*. *Development* **147**, dev184895 (2020).
43. Lee, K. et al. ESR2-HDA6 complex negatively regulates auxin biosynthesis to delay callus initiation in *Arabidopsis* leaf explants during tissue culture. *Plant Commun.* **5**, 100892 (2024).
44. Kim, J.Y. et al. Epigenetic reprogramming by histone acetyltransferase HAG1/AtGCN5 is required for pluripotency acquisition in *Arabidopsis*. *EMBO J.* **37**, e98726 (2018).
45. Lee, K. et al. *Arabidopsis* ATXR2 represses *de novo* shoot organogenesis in the transition from callus to shoot formation. *Cell Rep.* **37**, 109980 (2021).
46. Yin, R.L., Chen, R.Y., Xia, K.K. & Xu, X. A single-cell transcriptome atlas reveals the trajectory of early cell fate transition during callus induction in *Arabidopsis*. *Plant Commun.* **5**, 100941 (2024).
47. Zhang, T.Q., Chen, Y. & Wang, J.W. A single-cell analysis of the *Arabidopsis* vegetative shoot apex. *Dev. Cell* **56**, 1056–1074.e8 (2021).
48. Shahan, R. et al. A single-cell *Arabidopsis* root atlas reveals developmental trajectories in wild-type and cell identity mutants. *Dev. Cell* **57**, 543–560.e9 (2022).
49. Zhang, T.Q., Xu, Z.G., Shang, G.D. & Wang, J.W. A single-cell RNA sequencing profiles the developmental landscape of *Arabidopsis* root. *Mol. Plant* **12**, 648–660 (2019).
50. Matte Risopatron, J.P., Sun, Y.Q. & Jones, B.J. The vascular cambium: molecular control of cellular structure. *Protoplasma* **247**, 145–161 (2010).
51. Yu, Y. et al. Interneuron origin and molecular diversity in the human fetal brain. *Nat. Neurosci.* **24**, 1745–1756 (2021).
52. You, Y. et al. Systematic comparison of sequencing-based spatial transcriptomic methods. *Nat. Methods* **21**, 1743–1754 (2024).
53. Zhang, B.X., Zhang, H.L. & Xia, Y.J. Harnessing spatial transcriptomics for

advancing plant regeneration research. *Trends Plant Sci.* **29**, 718–720 (2024).
54. Sun, F.Y. et al. Single-cell omics: experimental workflow, data analyses and applications. *Sci. China Life Sci.* **68**, 5–102 (2025).
55. Wang, J.J. et al. Advances and applications in single-cell and spatial genomics. *Sci. China Life Sci.* **68**, 1226–1282 (2025).
56. Zhai, N., Pan, X., Zeng, M.H. & Xu, L. Developmental trajectory of pluripotent stem cell establishment in *Arabidopsis* callus guided by a quiescent center-related gene network. *Development* **150**, dev200879 (2023).
57. Bennett, T. et al. SOMBRERO, BEARSKIN1, and BEARSKIN2 regulate root cap maturation in *Arabidopsis*. *Plant Cell* **22**, 640–654 (2010).
58. Wendrich, J.R. et al. Vascular transcription factors guide plant epidermal responses to limiting phosphate conditions. *Science* **370**, eaay4970 (2020).
59. Farage-Barhom, S., Burd, S., Sonego, L., Perl-Treves, R. & Lers, A. Expression analysis of the *BFN1* nuclease gene promoter during senescence, abscission, and programmed cell death-related processes. *J. Exp. Bot.* **59**, 3247–3258 (2008).
60. Feng, Q.N. et al. Repressive ZINC FINGER OF ARABIDOPSIS THALIANA proteins promote programmed cell death in the Arabidopsis columella root cap. *Plant Physiol.* **192**, 1151–1167 (2023).
61. Cheng, Y.J. et al. Cell division in the shoot apical meristem is a trigger for miR156 decline and vegetative phase transition in *Arabidopsis*. *Proc. Natl. Acad. Sci. USA* **118**, e2115667118 (2021).
62. Desvoyes, B., Arana-Echarri, A., Barea, M.D. & Gutierrez, C. A comprehensive fluorescent sensor for spatiotemporal cell cycle analysis in *Arabidopsis*. *Nat. Plants* **6**, 1330–1334 (2020).
63. Yin, K. et al. A dual-color marker system for *in vivo* visualization of cell cycle progression in Arabidopsis. *Plant J.* **80**, 541–552 (2014).
64. Rosspopoff, O. et al. Direct conversion of root primordium into shoot meristem relies on timing of stem cell niche development. *Development* **144**, 1187–1200 (2017).
65. Wang, J.L., Sun, S.C. & Deng, H.K. Chemical reprogramming for cell fate manipulation: methods, applications, and perspectives. *Cell Stem Cell* **30**, 1130–1147 (2023).
66. Lee, L.R. et al. Glutathione accelerates the cell cycle and cellular reprogramming in plant regeneration. *Dev. Cell* **60**, 1153–1167.e6 (2025).
67. Zhang, T.Q. et al. A two-step model for de novo activation of *WUSCHEL* during plant shoot regeneration. *Plant Cell* **29**, 1073–1087 (2017).
68. Lee, S.J., Lee, M.H., Kim, J.I. & Kim, S.Y. Arabidopsis putative MAP kinase kinase kinases Raf10 and Raf11 are positive regulators of seed dormancy and ABA response. *Plant Cell Physiol.* **56**, 84–97 (2015).
69. Kohoutová, L. et al. The Arabidopsis mitogen-activated protein kinase 6 is associated with γ-tubulin on microtubules, phosphorylates EB1c and maintains spindle orientation under nitrosative stress. *New Phytol.* **207**, 1061–1074 (2015).
70. Favata, M.F. et al. Identification of a novel inhibitor of mitogen-activated protein kinase kinase. *J. Biol. Chem.* **273**, 18623–18632 (1998).
71. Zhang, M.M., Su, J.B., Zhang, Y., Xu, J. & Zhang, S.Q. Conveying endogenous and exogenous signals: MAPK cascades in plant growth and defense. *Curr. Opin. Plant Biol.* **45**, 1–10 (2018).
72. Zhu, Q.K. et al. A MAPK cascade downstream of IDA-HAE/HSL2 ligand-receptor pair in lateral root emergence. *Nat. Plants* **5**, 414–423 (2019).
73. Huang, R.F. et al. Noncanonical auxin signaling regulates cell division pattern during lateral root development. *Proc. Natl. Acad. Sci. USA* **116**, 21285–21290 (2019).
74. Zhou, Y. et al. Phosphatidic acid modulates MPK3- and MPK6-mediated hypoxia signaling in Arabidopsis. *Plant Cell* **34**, 889–909 (2022).
75. Zhou, F.L. et al. The MEKK1-MKK1/2-MPK4 cascade phosphorylates and stabilizes STOP1 to confer aluminum resistance in *Arabidopsis*. *Mol. Plant* **16**, 337–353 (2023).
76. Andreasson, E. & Ellis, B. Convergence and specificity in the *Arabidopsis* MAPK nexus. *Trends Plant Sci.* **15**, 106–113 (2010).
77. Zhai, D. et al. Reciprocal conversion between annual and polycarpic perennial flowering behavior in the Brassicaceae. *Cell* **187**, 3319–3337.e18 (2024).
78. Bae, S. H. et al. Stem cell activity is linked to a transient acquisition of pluripotency during callus proliferation. *Nat Commun* **17**, 6585 (2026).
79. Zwirner, S. et al. First-in-class MKK4 inhibitors enhance liver regeneration and prevent liver failure. *Cell* **187**, 1666–1684.e26 (2024).
80. Guan, J.Y. et al. Chemical reprogramming of human somatic cells to pluripotent stem cells. *Nature* **605**, 325–331 (2022).
81. Qin, H., Zhao, A.D. & Fu, X.B. Chemical modulation of cell fates: *in situ* regeneration. *Sci. China Life Sci.* **61**, 1137–1150 (2018).
82. Berenguer, E. et al. Inhibition of histone H3K9 methylation by BIX-01294 promotes stress-induced microspore totipotency and enhances embryogenesis initiation. *Front. Plant Sci.* **8**, 1161 (2017).
83. Bie, X.M. et al. Trichostatin A and sodium butyrate promotes plant regeneration in common wheat. *Plant Signal. Behav.* **15**, 1820681 (2020).
84. Martínez, Ó., Arjones, V., González, M.V. & Rey, M. Histone deacetylase inhibitors increase the embryogenic potential and alter the expression of embryogenesis-related and HDAC-encoding genes in grapevine (*Vitis vinifera* L, cv. Mencía). *Plants* **10**, 1164 (2021).
85. Valero-Rubira, I. et al. New epigenetic modifier inhibitors enhance microspore embryogenesis in bread wheat. *Plants* **13**, 772 (2024).
86. Wójcikowska, B. et al. Trichostatin a triggers an embryogenic transition in Arabidopsis explants via an auxin-related pathway. *Front. Plant Sci.* **9**, 1353 (2018).
87. Yang, W.T. et al. Peptide REF1 is a local wound signal promoting plant regeneration. *Cell* **187**, 3024–3038.e14 (2024).
88. Lee, H.G. et al. Adenosine monophosphate enhances callus regeneration competence for *de novo* plant organogenesis. *Mol. Plant* **16**, 1867–1870 (2023).
89. Clough, S.J. & Bent, A.F. Floral dip: a simplified method for *Agrobacterium*-mediated transformation of *Arabidopsis thaliana*. *Plant J.* **16**, 735–743 (1998).
90. Zhang, T.Q. et al. An intrinsic microRNA timer regulates progressive decline in shoot regenerative capacity in plants. *Plant Cell* **27**, 349–360 (2015).
91. Zhang, K. et al. A convenient, rapid and efficient method for establishing transgenic lines of *Brassica napus*. *Plant Methods* **16**, 43 (2020).
92. Van Eck, J., Kirk, D.D. & Walmsley, A.M. Tomato (*Lycopersicum esculentum*). In: Wang, K. ed. Agrobacterium protocols. 2nd Edition. Totowa: Humana, 459–474 (2006).
93. Won, K.H. et al. A reliable regeneration method in genome-editable bell pepper 'dempsey'. *Horticulturae* **7**, 317 (2021).
94. Zhao, C.L. et al. Efficient and transformation-free genome editing in pepper enabled by RNA virus-mediated delivery of CRISPR/Cas9. *J. Integr. Plant Biol.* **66**, 2079–2082 (2024).
95. Jiang, Q.Z., Fu, C.X. & Wang, Z.Y. A unified *Agrobacterium*-mediated transformation protocol for Alfalfa (*Medicago sativa* L.) and *Medicago truncatula*. In: Kumar, S., Barone, P. & Smith, M. eds. Transgenic plants: methods and protocols. New York: Humana, 153–163 (2019).
96. Finley, T., Chappell, H. & Veena, V. *Agrobacterium*-mediated transformation of *Setaria viridis*, a model system for cereals and bioenergy crops. *Curr. Protoc.* **1**, e127 (2021).
97. Chen, Q.H., Chen, T.Y., Lin, Y.J. & Chen, H. Agrobacterium-mediated genetic transformation of japonica rice. *Bio-101* **2018**, e1010174 (2018).
98. Amezquita, R.A. et al. Orchestrating single-cell analysis with Bioconductor. *Nat. Methods* **17**, 137–145 (2020).
99. Germain, P.L., Lun, A., Garcia Meixide, C., Macnair, W. & Robinson, M.D. Doublet identification in single-cell sequencing data using *scDblFinder*. *F1000Res.* **10**, 979 (2022).
100. Kurihara, D., Mizuta, Y., Sato, Y. & Higashiyama, T. ClearSee: a rapid optical clearing reagent for whole-plant fluorescence imaging. *Development* **142**,

4168–4179 (2015).
101. Chen, S.F., Zhou, Y.Q., Chen, Y.R. & Gu, J. fastp: an ultra-fast all-in-one FASTQ preprocessor. *Bioinformatics* **34**, i884–i890 (2018).
102. Ewels, P., Magnusson, M., Lundin, S. & Käller, M. MultiQC: summarize analysis results for multiple tools and samples in a single report. *Bioinformatics* **32**, 3047–3048 (2016).
103. Kim, D., Langmead, B. & Salzberg, S.L. HISAT: a fast spliced aligner with low memory requirements. *Nat. Methods* **12**, 357–360 (2015).
104. Song, J.M. et al. BnPIR: *Brassica napus* pan-genome information resource for 1689 accessions. *Plant Biotechnol. J.* **19**, 412–414 (2021).
105. Han, H.Y. et al. Chromosome-level genome assembly of *Solanum pimpinellifolium*. *Sci. Data* **11**, 577 (2024).
106. Li, H. et al. The sequence alignment/map format and SAMtools. *Bioinformatics* **25**, 2078–2079 (2009).
107. Cheng, C.Y. et al. Araport11: a complete reannotation of the *Arabidopsis thaliana* reference genome. *Plant J.* **89**, 789–804 (2017).
108. Liao, Y., Smyth, G.K. & Shi, W. featureCounts: an efficient general purpose program for assigning sequence reads to genomic features. *Bioinformatics* **30**, 923–930 (2014).
109. Love, M.I., Huber, W. & Anders, S. Moderated estimation of fold change and dispersion for RNA-seq data with DESeq2. *Genome Biol.* **15**, 550 (2014).
110. Stephens, M. False discovery rates: a new deal. *Biostatistics* **18**, 275–294 (2017).
111. Yu, G.C., Wang, L.G., Han, Y.Y. & He, Q.Y. clusterProfiler: an R package for comparing biological themes among gene clusters. *OMICS* **16**, 284–287 (2012).
112. Cooper, L., Elser, J., Laporte, M.A., Arnaud, E. & Jaiswal, P. Planteome 2024 Update: reference ontologies and knowledgebase for plant biology. *Nucleic Acids Res.* **52**, D1548–D1555 (2024).
113. Greene, D., Richardson, S. & Turro, E. ontologyX: a suite of R packages for working with ontological data. *Bioinformatics* **33**, 1104–1106 (2017).
114. Wang, S.S. et al. NAguideR: performing and prioritizing missing value imputations for consistent bottom-up proteomic analyses. *Nucleic Acids Res.* **48**, e83 (2020).
115. Ritchie, M.E. et al. *limma* powers differential expression analyses for RNA-sequencing and microarray studies. *Nucleic Acids Res.* **43**, e47 (2015).
116. O'Shea, J.P. et al. pLogo: a probabilistic approach to visualizing sequence motifs. *Nat. Methods* **10**, 1211–1212 (2013).
117. Schwartz, D. & Gygi, S.P. An iterative statistical approach to the identification of protein phosphorylation motifs from large-scale data sets. *Nat. Biotechnol.* **23**, 1391–1398 (2005).

ADDITIONAL INFORMATION

Supplementary information The online version contains supplementary material available at https://doi.org/10.15302/vita.2026.10.0086.

Correspondence and requests for materials should be addressed to Jia-Wei Wang.

Reprints and permission information is available at https://www.vita-journal.com/.

© The Author(s) 2026. Published by Higher Education Press. This is an Open Access article distributed under the terms of the CC BY license (https://creativecommons.org/licenses/by/4.0/).